



Hectorite: Synthesis, modification, assembly and applications

Jing Zhang, Chun Hui Zhou, Sabine Petit, Hao Zhang

► To cite this version:

Jing Zhang, Chun Hui Zhou, Sabine Petit, Hao Zhang. Hectorite: Synthesis, modification, assembly and applications. Applied Clay Science, 2019, 177, pp.114-138. 10.1016/j.clay.2019.05.001 . hal-02363196

HAL Id: hal-02363196

<https://cnrs.hal.science/hal-02363196>

Submitted on 2 Dec 2020

HAL is a multi-disciplinary open access archive for the deposit and dissemination of scientific research documents, whether they are published or not. The documents may come from teaching and research institutions in France or abroad, or from public or private research centers.

L'archive ouverte pluridisciplinaire **HAL**, est destinée au dépôt et à la diffusion de documents scientifiques de niveau recherche, publiés ou non, émanant des établissements d'enseignement et de recherche français ou étrangers, des laboratoires publics ou privés.

Hectorite: Synthesis, Modification, Assembly and Applications

Jing Zhang^a, Chun Hui Zhou^{a,b,c*}, Sabine Petit^d, Hao Zhang^a

^a Research Group for Advanced Materials & Sustainable Catalysis (AMSC), State Key Laboratory Breeding Base of Green Chemistry-Synthesis Technology, College of Chemical Engineering, Zhejiang University of Technology, Hangzhou 310032, China

^b Key Laboratory of Clay Minerals of Ministry of Land and Resources of the People's Republic of China, Engineering Research Center of Non-metallic Minerals of Zhejiang Province, Zhejiang Institute of Geology and Mineral Resource, Hangzhou 310007, China

^c Qing Yang Institute for Industrial Minerals, You Hua, Qing Yang, Chi Zhou 242804, China

^d Institut de Chimie des Milieux et Matériaux de Poitiers (IC2MP), UMR 7285 CNRS, Université de Poitiers, Poitiers Cedex 9, France

Correspondence to: Prof. CH Zhou E-mail: clay@zjut.edu.cn; chc.zhou@aliyun.com

Abstract

Hectorite ($\text{Na}_{0.6}\text{Mg}_{2.7}\text{Li}_{0.3}\text{Si}_4\text{O}_{10}(\text{OH})_2$) is a trioctahedral clay mineral with peculiar cation exchange capacity, surface reactivity and adsorption, and easy delamination in water into individual nanolayers, which can then re-assemble in various ways. The aqueous dispersion of hectorite exhibits exclusive rheological and thixotropic properties. The paper reviews recent progress in the synthesis, modification, assembly and applications of hectorite. The present methods for synthesizing hectorite are hydrothermal synthesis, melt synthesis and structure-directed synthesis. Modification of hectorite can be made by ion exchange, intercalation, pillaring and grafting. Layer-by-layer assembly, template assembly and hierarchical assembly have been used to form a variety of hectorite-containing hybrids and nanocomposites such as films, membranes, capsules and Janus nanoparticles. Hectorite and hectorite-derived materials can be used as adsorbents, catalysts, fluorescent reporters, hydrogels, and biomaterials. Literature survey has indicated that hectorite has been successfully used as rheological and thixotropic materials, and are being developed to be used in battery, fluorescent reporters, drug vehicles and tissue engineering.

Keywords: Hectorite; Synthesis; Modification; Assembly; Adsorption; Hydrogel; Biomaterials

1. Introduction

Hectorite is a natural layered magnesium-lithium silicate, and it is a trioctahedral clay mineral with an ideal chemical formula of $\text{Na}_{0.6}\text{Mg}_{2.7}\text{Li}_{0.3}\text{Si}_4\text{O}_{10}(\text{OH})_2$ in the smectite group. The layered structure of hectorite is composed of Si-O-Mg(Li)-O-Si- layers separated by hydrated cations (e.g. Na^+ , Li^+) in the interlayer space. Each layer (ca. 0.96 nm thin) consists of two Si-O-Si tetrahedral sheets sandwiching a Mg-O-Li octahedral sheet in a so-called 2:1 arrangement (**Fig. 1a**). The adjacent negatively-charged 2:1 layer is fixed by positively-charged interlayer cations and by hydrogen bonding between water molecules coordinated to interlayer cations and basal oxygen atoms of tetrahedral sheets. The partly isomorphous substitution of Li^+ for Mg^{2+} in the octahedral sheets cause negative charges that is compensated by interlayer cations in the

interlayer space and the interlayer cations are exchangeable. Hectorite nanolayers possess anisotropic distribution of charge in the layer: negative charges on the basal faces and positive charges on the edges (**Fig. 1a**). The amphoteric groups (Mg-O, Li-O, and Si-O) at the broken edge of the crystals is protonated (Mg-OH_2^+ , Li-OH_2^+ , and Si-OH_2^+) or deprotonated (Mg-O^- , Li-O^- , and Si-O^-), depending on the pH (Bourlinos et al., 2004). Hectorite has cation exchange capacity (CEC) ranged from 50 to 150 mmol/100g over the pH range of 6 to 13 (Delavernhe et al., 2018), and specific surface area about $350\text{m}^2/\text{g}$ (Hegyesi et al., 2017).

Fig. 1.

Hectorite can spontaneously swelling and then delaminate in water (Gaharwar et al., 2013). Many dispersed individual layers in water can then form the structure of “house-of-cards” (Fig. 1b). Such randomly oriented “house-of-cards”, and its stacking can be destroyed and aligned under a shearing force. Under static condition, an aqueous dispersion of delaminated hectorite can form sol or hydrogel with a 3D network, primarily dependent on the concentration, media and electrolyte (Iwase et al., 2018; Lezhnina et al., 2012). As such, the aqueous dispersion of hectorite exhibits superior and tunable rheological and thixotropic properties (Phuoc et al., 2009; Tan et al., 2014).

Hectorite deposits in nature are rare. Due to the geological environments and conditions, natural hectorite at different deposits has variable crystallinity and various impurities, limiting the use of hectorite. Hectorite is one of easily synthesized clay minerals by a hydrothermal process in the laboratory and in industry (Strese and Hofmann, 1941; Granquist and Pollack, 1959; Decarreau, 1980; Zhang et al, 2010). Laponite[®], a kind of synthetic hectorite, has been produced on a large scale and widely used (The name Laponite[®] was introduced by the Laporte Industries decade ago). Ideally, well-synthetic hectorite is homogeneous in composition and crystallinity by controlling the hydrothermal process. Besides, studies have indicated that hectorite-like solid can be synthesized by a solid-state reaction or template synthesis. In this way, the nanolayer can be controlled to have a high aspect ratio or to be conducive to form porous structure. In addition, the reactive groups on the surface and the edge of hectorite allow hectorite to be functionalized by grafting. The functionalized hectorite can be further assembled with other molecules and

nanomaterials to form nanohybrids or nanocomposites by layer-by-layer assembly, template assembly or hierarchical assembly.

New discoveries and technologies about hectorite emerged constantly, and one can say that the excitement of hectorite continues unabated in the recent decade (**Fig. 2a**). Traditionally, hectorite can be used as adsorbent, catalytic and rheological additives. More recently, hectorite is often seen to be used in the fields of advanced analytic and optical, diagnostic, medical materials and tissue engineering (**Fig. 2b**). In particular, new technologies for synthesis, modification and assembly of hectorite is paving the way for many new applications of hectorite.

Fig.2.

2. Synthesis

2.1 Hydrothermal synthesis

Since Strese and Hofmann (1941) successfully synthesized hectorite-like solid from aqueous solution at reflux temperature for the first time, a hydrothermal process has been commonly used for synthesizing hectorite (**Table 1**). Though this technology of synthesis of hectorite has become much mature, cleaner production of hectorite with more energy-efficiency is still need. In addition, synthetic hectorite with new structures such as ordered heterostructures (Stöter et al., 2014) and Janus nanoparticles (Stöter et al., 2016) also rekindles the development of the methods to synthesize hectorite.

Table 1

2.1.1 Formation mechanism

It has been generally believed that hectorite. nucleation is initiated from brucite sheets. To be specific, the nuclei occur starting with the condensation of silicate tetrahedral Si-O blocks onto

brucite sheets (**Fig. 3a, eq 1**). It has been ever observed that during the synthesis, the more crystalline brucite is yielded, the larger amount of crystalline hectorite is produced (Vicente et al., 2009). In addition, it is found that some of these initial nuclei are redissolved and recondensed to form nuclei of hectorite (Okada et al., 2012; Okada et al., 2015a; Okada et al., 2016b). In the process, the added Mg^{2+} and Li^+ form water-soluble Mg-Li double hydroxide (**Fig. 3c, eq 3**). Such brucite-like Mg-Li sheets act as initial species for nucleation and growth. The sheets are also the precursors of the octahedral sheet of the resultant hectorite.

The silica (SiO_2) on the surface of SiO_2 precipitates or solids dissolves into the aqueous phase to form silicate anions SiO_3^{2-} (**Fig. 3b, eq 2**). When approaching the Mg-Li hydroxide, the silicate anions condense and meanwhile react with on the Mg-Li double hydroxide to form nuclei. During nucleation and growth of hectorite, dehydroxylation mainly occurs. Finally, the nuclei and tiny crystallite of 2:1 layered Mg-Li-silicates, namely hectorite, grows in a two-dimensional way (**Fig. 3d, eq 4**). The dissolved silica is continuously consumed with the formation of hectorite. The compositional balance of silica, LiF, and MgCl_2 should be responsible for the heterogeneous nucleation (Okada et al., 2015b; Okada et al., 2016a). Whatever the process involved, after the crystallization is complete, layer-layer stacking and agglomeration of nanoparticles takes place commonly (Carrado et al., 2002).

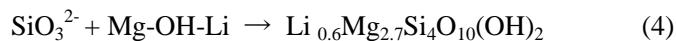
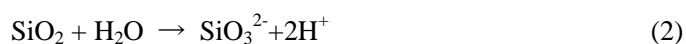


Fig.3.

Yet it is worth arguing if the preceding formation of brucite sheet are necessary step in the formation of hectorite. For example, A process using coprecipitated gels (**eq 5**) with further or immediate addition of LiF (or LiCl) (**eq 6**) followed by hydrothermal treatment also produced hectorite (Decarreau, 1980; Decarreau et al., 2012). In the studies, freshly coprecipitated gels

appeared to contain nanoparticles (less than 0.1 μm in diameter) and the nanoparticles aggregated more or less. The freshly coprecipitated gels were composed of nuclei which had the structure of hectorite layers (Decarreau, 1980). OH^- released during reaction (eq 5). Owing to H^+ release into solution (eq 6), a decrease of pH with the time of hydrothermal treatment. After reaction of nucleation, the pH was between 9 and 10 (Carrado, 2000)



F^- ions are viewed as favorable mineralizing agents during the hydrothermal synthesis of hectorite. Such mineralizing agents could play a role in regulating dissolution, hydrolysis, condensation, dehydroxylation and thereby nucleation and growth of hectorite crystals. In particular, it has been suggested that F^- ions promote the dissolution and hydrolysis of the silica (Okada et al., 2015a). Moreover, it has been revealed that the F^- ions partly replaced the hydroxyl groups in the layer and created defects in the lattice (Jaber and Miehé-Brendlé, 2008). Such F^- in the framework of hectorite layers inhibit the interaction of neighboring hydroxyls to produce water, as proved by the enhanced thermal stability of fluorohectorite. Finally, it is also revealed that the presence of F^- ions during the synthesis resulted in enhanced layer stacking in the direction of the c^* -axis in the heterogeneous nucleation and growth of hectorite (Okada et al., 2015a).

2.1.2. Insights into reaction conditions

The composition and purity of synthetic hectorite can be controlled by judiciously choosing the molar ration of Si:Mg:Li and the hydrothermal reaction conditions (Zhou et al., 2010). The size distribution of synthetic hectorite, which is inherently to the nucleation and growth of synthetic hectorite crystals, can also be tuned primarily by crystallization time, hydrothermal temperature, pH value and heating. It is also influenced by the methods of heating and stirring, for example microwave heating and ultrasonication (Table 1).

Synthetic hectorite is usually produced from crystallizing an aqueous mixture of LiF and/or LiCl, Mg(OH)₂ and SiO₂ at high-temperature under reflux conditions in an open system or under autogenic pressure in an autoclave. Generally, the molar ratio of reactants for synthetic hectorite is set to match the ideal composition of natural hectorite Na_{0.66}[Li_{0.66}Mg_{5.34}Si₈O₂₀(OH)₄]. But the ions from the reactants might play a multiple role in the formation of hectorite. Typically, Li⁺ substitute for some of octahedral Mg²⁺, leading to layer charge (Makoto et al., 2008). Decarreau et al. (2012) recently revealed that the Li content of hectorite increased with the Li⁺ concentration in the solution and proposed a partition coefficient D_{Li} with a general expression $D_{Li} = \frac{Li_{hectorite}}{Li_{solution}}$ and $\log D_{Li} = -1.319 \cdot 10^3/T + 5.5 (Li_{solution})^{-0.0806}$ (T=343-453K). Accordingly, the Li/Mg molar ratio of reactants significantly influence the layer charge density (LCD) and the CEC due to the variable isomorphous substitution (Karmous et al., 2009; Okada et al., 2015b). In addition, it has been found that the amount of LiF can also affect the size of the hectorite crystals, the surface area and pore size of the synthetic hectorite (Pawar et al., 2013).

Various metal-substituted hectorite-like solid have been synthesized (**Table 1**). Well-crystallized Zn-hectorite (Na_{0.4}(Li_{0.4}Zn_{2.6})Si₄O₁₀(OH)₂·nH₂O) were obtained at 373K (Spagnuolo, 2004). Cu, Ni, Mn and Co-hectorite can only be hydrothermally synthesized under the conditions of more crystallization time and higher temperature (around 473K) (Spagnuolo, 2004), due to the lower electronegativity (Ni, Mn and Co electronegativity: 1.91;1.55;1.8) (Higashi et al., 2007). The electronegativity of ions is directly related to the ionic radius. Besides, actinides and lanthanides elements such as Cm(III) (Brandt et al., 2007), Eu(III) (Finck et al., 2008) and Am(III) (Finck et al., 2015) can also replace part of Mg²⁺ in the octahedral sheet. However, a study from Thien et al. (2010) suggested that Cd²⁺ and Pb²⁺ cannot enter octahedral sheets, because the ions are too large to be accommodated within the magnesium-lithium silicate layer.

For the hydrothermal synthesis of hectorite, heating the reactor to 373K-453K is required. At high temperature, well-crystallized hectorite can form in a short time, typically 2h at 473K (Iwasaki, 1989). The reaction time affects the crystallinity and the particle size of hectorite product. The lattice structure of synthetic hectorite is most possibly grown on the verge of the amorphous reactants. With increasing aging time, the crystallinity of hectorite then increases (Carrado et al., 2015). When less crystallization time (4h) is used, the resultant hectorite has

smaller particle size and exhibits narrow size distribution with poor crystallinity (Vicente et al., 2009). Hectorite has better crystallinity with larger particle size and higher thermal stability when the crystallization time is long enough (usually, several days)(Sánchez et al., 2013b). Decarreau et al. (2012) revealed that a chemical steady-state (SiO_2 , Na_2O , MgCl_2 as starting gel with LiCl) was reached after 4 weeks at 423K and after 2 months at 443K and 463K. For shorter time (some days at 453K), the 2-dimensional growth of synthetic hectorite along its (001) plane was preferred. In this way, the CEC and the aspect ratio of the synthetic hectorite were then increased (Hai et al., 2018a). Therefore, the temperature and the time for the hydrothermal synthesis of hectorite should be optimized according to the desired features of the products.

Commonly, the hydrothermal reaction to produce hectorite occurs at pH 9-10 (Carrado, 2000). When pH value is higher than 11, much OH^- and the enhanced ionic strength may change the nature of precursor gel. In particular, the precipitation and crystallization of $\text{Mg}(\text{OH})_2$ does not occur. If pH is too low, $\text{Mg}(\text{OH})_2$ is dissolved (Sánchez et al., 2013b). In both cases, there is no $\text{Mg}(\text{OH})_2$ as the precursor of the octahedral sheet of hectorite. It is worth noting that hectorite could also be formed from stevensite after Li^+ migration into the vacant site upon dry heating (Petit et al, 2008). More recently, studies show that 2D hectorite-like layers can be scrolled to some degree to form nanotubes under hydrothermal conditions (Hai et al., 2018). Such nanotubes have large outer diameters in the range 100–200 nm and lengths of several micrometers.

2.1.3. Intensified processes

Conventional hydrothermal synthesis of hectorite is conducted at high temperatures for long aging time. It is time-consuming and energy-intensive. Hence, in this context, a rapid process is desired. Microwave heating and ultrasound technology have been used for intensifying the synthesis of hectorite. Microwave oven acts as heater in the hydrothermal synthesis of hectorite. Microwave can provide fast and homogeneous heating and increase the movement rate of reactant molecules. As a result, the crystallization time of synthetic materials is significantly reduced (Vicente et al., 2009). Besides, microwave treatment leads to aggregation with the edge-to-face connections of hectorite nanoparticles, forming a stable structure with mesoporosity (Vicente et al.,

2010; Sánchez et al., 2013b). This mesoporous hectorite shows narrow pore size distribution and is more resistant to dehydroxylation than corresponding microporous hectorite.

Ultrasonic wave can be used to intensify the mixing of reactants and thus can create more homogeneous mixture of starting materials or precursors of hectorite (Sánchez et al., 2013b). Accordingly, the resultant synthetic hectorite, possesses fewer vacancies in the lattice, lower surface areas and better constructed layers, compared with the synthetic hectorite made by conventional hydrothermal synthesis. For instance, a better incorporation of magnesium and lithium in the octahedral sheet has been achieved by the ultrasound-assisted synthesis (Sánchez et al., 2013a).

2.1.4. Structure-directed synthesis

Organic moieties can be covalently introduced into hectorite by using an organosilane as a silica source $[\text{RSi}(\text{OR}')_3]$, where R stands for alkyl groups and R' for methoxy or ethoxy groups]. The method is called *in-situ* synthesis of organo-hectorite and is different from post-grafting of hectorite with organic groups. The silicon atoms of the tetrahedral sheets are covalently bounded to the organic groups present in the interlayer space (**Fig. 4a**). For example, tetraalkoxysilane and organo-trialkoxysilane have been used as the silicon sources. After crystallization under hydrothermal conditions, the moieties of organosilane are covalently attached to $-\text{O}-\text{Si}-\text{O}-$ in the interlayer surface of hectorite (Whilton et al., 1998; Carrado et al., 2001). When the organosilane is used, the crystallization rate of hectorite by *in-situ* synthesis is approximately twice as much as the one when SiO_2 is used (Carrado et al., 2002). This is because the inorganic silica gel usually needs longer time to dissolve and form sol as the silicate precursor species. By contrast, that the silica sol is immediately available when a silane is used.

Besides acting as blocks in synthetic hectorite, organic species, for example alkyl imidazolium cations, can also act as structure-directing agents or templates (**Fig. 4b**). As a whole, the addition of structure-directing agents into the mixture of reactants aim at producing micro- to mesoporous hectorite (Joshi et al., 2011). The pore diameters depend on the size of organic cation and the amount in the mixture for the hydrothermal reaction. Dependent upon the concentration in water, organic cations can self-assemble and then form different structured supramolecules which

act as template. Typically, for such structure-directed synthesis, the alkyl chain length has the effect on the specific surface area, pore size and pore volume of the resultant hectorite. For example, mesoporous hectorites have been synthesized by hydrothermal crystallization of gels containing silica, magnesium hydroxide, lithium fluoride, and 1-butyl-3-methylimidazolium bromide (BMI), 1,3-didecyl-2-methylimidazolium chloride (DDMI) or 1-decyl-3-methylimidazolium chloride (DMI) as structure-directing agents at 723K for 48 h (Pawar et al., 2009; Joshi et al., 2011). After calcination, the organic species were burnt and removed and an inorganic porous hectorite with a narrow pore size distribution in the mesoporous range of 3.4 to 5.5 nm was achieved. The pore diameters were found dependent on the molecular mass and size of the imidazolium cations and, to some extent, on its amount used. Tetraphenylphosphonium bromide was also employed as template for producing porous synthetic hectorite (Sethia et al., 2014). The porous hectorite has the single point adsorption total pore volumes of 0.33 cm³/g and a specific surface area of 384 m²/g. Besides, structure-directing synthesis is used to produce hectorite with large nanolayers and good dispersibility in organic solvent (Carrado et al., 1997).

Fig.4.

Generally, mild conditions are required to ensure the structural integrity of organic moieties when the structure-directing synthesis and the *in-situ* synthesis is conducted (Carrado, 2000). By contrast, a hard template can endure heating which are usually needed for hydrothermal reactions. Specifically, by using carbon spheres as hard template, hollow microspheric hectorite has been synthesized as demonstrated by Sawant et al. (2014). The carbon spheres were introduced to reaction system by coating with Mg(OH)₂. The synthetic, hollow and microspheric hectorite was obtained by the calcination of hectorite-coated carbon spheres at 773K for 2h at the heating rate of 1K/min. The morphology and surface area of hollow and microspheric hectorite can be controlled by the amount and size of carbon spheres. In this way, hierarchically hectorite-based materials have been achieved. Such hard-template synthesis methodology opens new avenues to make many kinds of advanced hectorite-based materials with distinct properties and applications.

2.2 Melt synthesis

A recent study from Christidis et al. (2018) discovered that hectorite products by a hydrothermal process contain up to 25% non-swelling kerolite layers and stevensite, and should be characterized as mixed layer phases. In addition, it has been found long ago that for a hydrothermally prepared hectorite, the charge density is rather heterogeneous and the intracrystalline reactivity is non-uniform (Decarreau et al., 1992). This non-uniformity might result from the solid solution capability of the 2:1 layered silicate structure of hectorite at low temperatures (373-523K) (Muller et al., 1997; Josef et al., 2001). Several studies indicated that melt synthesis, a solid state reaction which the temperature exceeding 1000 K, can provide a solution to the problems and is conducive to producing pure hectorite product with homogeneous charge density (Kalo et al., 2012a; Kalo et al., 2012b; Stöter et al., 2013; Christidis et al., 2018).

Josef and his co-workers (2001) demonstrated a melt synthesis of fluorohectorite in gas-tight molybdenum crucibles. The reactants, including SiO_2 , MgO and three kinds of fluorides (LiF , MgF_2 , NaF), were mechanically rotated during synthesis to assure continuous mixing of the melt at 1823-2373K. However, the cost of the non-reusable crucibles, the limitations of productivity in batch sizes, and the necessity of using highly pure anhydrous chemicals are problematic. Later, Josef's group developed large scale melt synthesis which undergoes at 1538K under argon flow in an open crucible to produce Na^+ -fluorohectorite with superb charge homogeneity and particle size (Kalo et al., 2010). In order to maintain a low vapor pressure of volatile fluorides and sustain a low silica activity, a glass ($\text{Na}_2\text{O-Li}_2\text{O-SiO}_2$) precursor was used as a fluxing agent. The fluxing agent can inhibit the formation of silicon fluoride gases and promotes the lithium fluoride solubility in the melt. That is why the product showed a superb homogeneity of the charge density, even though this open system leads to unavoidable gradients in composition.

In addition, melt synthesis can lead to ordered stacking products. The details of crystal structures for both the one-layer and the two-layer hydrates of hectorite have been uncovered by using the samples from melt synthesis (Kalo et al., 2012a). The cations in the interlayer space of hectorite are located off the central plane and exist in a nine-fold coordination. Namely, a cation coordinated with six basal oxygen atoms and three water molecules. The stacking order of the

adjacent 2:1 layer is determined by hydrogen bonding of the water molecules to another tetrahedral sheet.

Furthermore, through melt synthesis, synthetic hectorite with very large aspect ratios (> 10,000) can be obtained. Kalo et al. (2012b) reported the synthesis of lithium–fluorhectorite at 1623K with silicic acid hydrate, MgF_2 and excess Li_2O – 2SiO_2 glass. This melt-synthesis yielded Li-hectorite has variable layer charge, particle diameter and reactivity increased concomitantly with increasing layer charge. Besides, Stöter et al. (2013) found that long-term annealing can produce Na^+ -fluorhectorite with improved swelling property. The Na^+ -fluorhectorite can delaminate into nanolayers of 1 nm in thickness with an aspect ratio of 18 000.

In the melt synthesis hectorite, Li might be introduced to both octahedral and interlayer sites. "In a recent study, Christidis et al (2018) suggested that subsequent annealing of the melt-derived fluorinated hectorite can cause migration of the exchangeable Li into the vacancy of octahedral sheets due to the Hofmann-Klemen effect (Hofmann and Klemen, 1950). As these Li^+ directly balanced the negative charges in the layer, the overall layer charge is decreased and the amount interlayer cations become less (Christidis et al., 2018).

3 Modification

Hectorite possesses several kinds of active sites: the interlayer sites, surface sites, edge sites and inter-particle sites (**Fig. 5**). These active sites can react or interact with other components and hence can be tactically used to modify hectorite. The modification can be conducted by acid treatment, ion exchange, intercalation, grafting and pillaring (**Table 2**).

Acid treatment inherently leads to the controlled, ion exchange, partial dissolution or breakage of hectorite because the hectorite attacked by acid and the products are called acid-activated hectorite. The mild acid treatment of hectorite yields a protonated hectorite (Tkáč, 1994; Breen and Komadel, 1995). If the acid is strong enough the proton severely attacks the oxygen sites, which connecting the octahedral and tetrahedral sheets on the edge of the faces (Bickmore et al., 2001; Komadel, 2016) and partly damage the structure of hectorite. Consequently, the surface acidity, specific surface area and average pore volume of the acid-activated hectorite are increased (Franco et al., 2016). Typically, such acid-activated hectorite

as a catalyst exhibit remarkable acid catalytic activity (Komadel et al., 1997). Acid treatment can also act as a pretreatment of hectorite for further modification.

Organic or inorganic cations as exchangeable cations partly or completely replace exchangeable cations in interlayer space of hectorite. In this way, guest cations can be intercalated into in interlayer space of hectorite. When bulky inorganic ions can be intercalated into in interlayer space of hectorite, after calcination the hybrids can be converted into pillared hectorite. Macromolecules can also be inserted into the interlayer space of hectorite to form the intercalated composites (Kotal and Bhowmick, 2015). Besides, the silanol and M-OH groups on the edge of hectorite can react with functional reactive groups of some organic reagents and form a class of grafted hectorite hybrids. Of these modification methods, ion exchange and grafting are more extensively used over the past few decades.

Fig.5.

Table 2

3.1. Ion exchange and intercalation

The negative charge on the layer of hectorite is compensated by cations, usually Na^+ and/or Li^+ , in the interlayer space of hectorite. The electrostatically attracted cations can be replaced by other cations by an exchange reaction. Both organic and inorganic cations can be properly selected as the exchangeable cations to partly or completely replace the original exchangeable cations of hectorite.

A kind of mixed-cation heterostructures of synthetic Na^+ -fluorohectorite with an K^+ in one interlayer space and Na^+ in one interlayer space in an alternating interstratification pattern can be obtained by the partial cation-exchange reaction between synthetic Na^+ -fluorohectorite and K^+ (Möller et al., 2010). The largely different hydration enthalpies (Na^+ by K^+) led to the regular interstratification of hydrated ($d = 12.4 \text{ \AA}$) and nonhydrated ($d = 10.0 \text{ \AA}$) interlayers at 40% relative humidity(**Fig. 6**). Consequently, the original homogeneous charge density in the

interlayers of synthetic Na^+ -fluorohectorite was changed. The interlayer space with K^+ and the CEC of the collapsed nonhydrated (K^+) interlayers proved to be higher and the corresponding hydrated (K^+) interlayers become lower. This made the interlayers differentiated, allowing it to be selectively manipulated for fabricating bifunctional materials (Stöter et al., 2014; Stöter et al., 2015).

Fig.6.

Especially, the ordered heterostructure offers predetermined slippage planes, which can be easily cleaved or exfoliated (Walther and Müller, 2013). For example, after NH_4^+ exchange of Na^+ -hectorite, ordered heterostructure with alternating NH_4^+ non-hydrated interlayers and adjacent readily hydrated Na^+ interlayers are formed (Stöter et al., 2016). Such heterostructural hectorite can be converted into Janus nanoparticles (**Fig.7**). Through osmotic swelling and deprotonation, the bilayers can convert into Janus-type nanoparticles. Similarly, by controlled partial ion exchange, Na^+ -hectorite can also be converted into a one-dimensionally (1D)-ordered, regularly interstratified heterostructure with alternating Na^+ and n-butylammonium (C_4) interlayers (Daab et al., 2017). This heterostructure spontaneously delaminates uniformly into single layers upon being dispersed in water to form Janus nanoparticles.

Besides inorganic ions, organic cations can also be incorporated into the interlayer space of hectorite through an ion-exchange reaction. Organic cations, such as tallow-triethanol-ammonium (Awad et al., 2009), methyl trioctyl ammonium (Yu and Cebe, 2009), dimethyl dehydrogenated tallow ammonium (Velasco et al., 2007), trimethyl octadecyl ammonium (Dykes et al., 2010) have been used to modify hectorite. Typically, tetramethylammonium chloride (TMAC) dissociates into TMA^+ cations and Cl^- anions in aqueous medium. TMA^+ cations replace Na^+ in the interlayer space of hectorite (**Fig. 7a**) (Tan et al., 2014) to form TMA-hectorite. The organic-modified hectorite usually has improved organophilic and hydrophobic. It can delaminate to form monodispersed nanoparticles and organogel in an organic solvent (Wang et al., 2009). Depending on the type of the organic cations, and the packing density and chain length, the corresponding organo-hectorite exhibits different structure and properties (Hendrik et al., 2007). Small

organo-ammonium cations, such as tetraethylammonium (TEA^+) do not pack densely and generate empty nanospace in the interlayer space of hectorite due to the local charge repulsion and the stoichiometric balance of the charge (**Fig. 7c**) (Bracco et al., 2008). The methylene and methyl hydrogens of TEA^+ interacted with silicon of hectorite. It is well documented that the chain length of organic cations significantly plays a role in the expansion of the interlayer spacing of organohectorite. Compared with the TEA-hectorite, Hectorite intercalated with octadecylammonium ions (ODA-hectorite) has larger interlayer spacing (**Fig. 7f**). Nevertheless, long alkyl chains could completely occupy the interlayer space of hectorite, thereby preventing porosity (**Fig. 7d and e**). In addition, the amount of organo species introduced into the interlayer space of hectorite are crucial to the arrangement of organo cations and then to the porosity. For example, upon the amount of MV^{2+} , MV^{2+} -hectorite (MV^{2+} : 1,1'-dimethyl-4,4'-bipyridinium) has a pore volume of 0.055-0.088 cm^3/g and an average pore size of 0.70-1.43 nm (Okada, 2010).

The conventional process to produce organohectorite is relatively costly and tedious because it involves multistep treatments (Yu et al., 2014). Typically, hectorite is dispersed in water and the organic compounds are dissolved in water. Then the two are mixed for an ion exchange reaction so that quaternary ammonium cations were gradually intercalated into the interlayer space of hectorite. After reaction, the resultant solid need be separated, washed with water and dried upon heating. Such a tedious process is energy-intensive. Moreover, it leads to a large amount of wastewater with excess inorganic ions (e.g. Na^+ , Li^+ , Br^- , Cl^-) and organic cations in it. Therefore, development of a simple and clean process to produce organohectorite is much necessary in practice. Ion exchange reaction between the interlayer cations of hectorite with various phosphonium and ammonium cations have been successfully carried out in supercritical CO_2 (Naveau et al., 2009). After reaction and CO_2 evacuation, the organo-hectorite can be directly recovered as a fine powder. Besides, the phosphonium-hectorite is found to be more thermally stable than the conventional alkylammonium- hectorite.

Fig. 7.

3.2. Pillaring

Pillaring describes a process of transforming a layered compound into a thermally stable micro- and/or mesoporous material with the formation of pillars and the retention of the layer structure (Tsapatsis and Maheshwari, 2008). Pillared hectorite is usually obtained by exchanging the interlayer cations of hectorite with polymeric or oligomeric hydroxymetal cations, followed by converting the hydroxymetal cations into stable oxide pillars in the interlayer space of hectorite upon calcination. The resultant pillared hectorite is micro- and/or mesoporous and thermally stable to some extent (Storaro et al., 1996). Obviously, such pillars can tune the pore size. Pillared hectorite can possess a two-dimensional long range order of pillars and then exhibits a narrow pore size distribution. To achieve this, the hectorite and the pillaring process must be well controlled (Guerra et al., 2008). In addition, Pillars, as building blocks of pillared hectorite, provide additional inner surface and chemical functionality. Hence, selecting pillaring agents and creating different pillars are essential to the physical and chemical properties of the pillared hectorite (Okada and Ogawa, 2003). For example, FeO_x-pillared hectorite was successfully synthesized by intercalation of iron precursors (FeCl₃), followed by calcinations at 573K (Trikitiwong et al., 2014). The surface area was increased from 57.11 m²/g for hectorite to 122.30 m²/g for FeO_x-pillared hectorite. Besides, both weak acid sites and strong acid sites were remarkably increased.

Generally, the organic pillars bridge the interlayer space in a defined way by penetrating into the hollows on the corrugated silicate surfaces on both sides of the interlayer space. In this way, the hexagonal cavities are forced to be arranged on the opposite each other. But this is not a general law. For example, it has been reported that when large organic pillars, such as 1,4-diazabicyclo[2.2.2]octane (DABCO) molecules, were made, the stacking order of the host Cs⁺-hectorite was still preserved and the resultant microporous material does not suffer from stacking faults (Stocker et al., 2008). Besides, when the layer charge of K⁺-hectorite was reduced to $x < 0.48$ per formula unit (pfu) by utilizing the Hofmann-Klemen effect, the pillared hectorite show a significant increase in both micropore volume and pore width (Hofmann and Klemen, 1950; Herling et al., 2012) (**Fig. 8a and 8b**). By pillaring K⁺-hectorite with

N,N-dimethyl-1,4-diazabicyclo[2.2.2]octane dication ($\text{Me}_2\text{DABCO}^{2+}$), the pore volume ($<10 \text{ \AA}$) of Me_2DABCO -hectorite increases to $0.150 \text{ cm}^3/\text{g}$ from $0.077 \text{ cm}^3/\text{g}$ of K^+ -hectorite (Herling et al., 2012). By contrast, by pillaring K^+ -hectorite with rhodium-tris-2,2-bipyridin trication ($\text{Rh}(\text{bpy})_3^{3+}$), the pore volume of $\text{Rh}(\text{bpy})_3$ -hectorite can be increased to $0.164 \text{ cm}^3/\text{g}$ from $0.112 \text{ cm}^3/\text{g}$ of K^+ -hectorite. The spherical shape of $\text{Rh}(\text{bpy})_3^{3+}$ can create a larger interlayer spacing and the higher charge of $\text{Rh}(\text{bpy})_3^{3+}$ as the pillar make the pillared hectorite need fewer, d more pillars separated from each other, thereby further creating larger available space (**Fig. 8c**). Clearly, the shape and size of the pores of pillared hectorite are not only determined by the layer charge of the hectorite, but also depended on the charge, size, and shape of the pillars.

Fig. 8.

3.3. Grafting

Hectorite has reactive hydroxyl groups on the edges in the form of Si-OH and $\text{Mg}(\text{Li})\text{-OH}$ groups, and inside the layer in the form of Mg-OH or Li-OH groups. In particular, the reactive silanol groups are readily accessible to functional groups of organic agents. It is now also found that the high negative charge of hectorite (approximately 700 electron charges pfu) effectively facilitates the nuclear substitution reaction in which hectorite reacts with alkylsilane to generate new O-Si bonds, as called a grafting process by silylation (Delavernhe et al., 2018). Such silylation of hectorite allows the formation of $-\text{Si-O-R-O-Si}-$ linkages between hectorite nanoparticles (Daniel et al., 2008).

The grafting between hectorite and hydrophobic silane groups takes place mainly on the external surface, while the interlayer space remains nearly intact (Yang et al., 2013; González et al., 2017). When the silylating agent was grafted on the edges of the hectorite layers, the individual hectorite nanolayers was chemically locked into irreversibly stacks (Norma et al., 2004). Recently, Yang et al. (2013) successfully fabricated amphiphilic hectorite with hydrophobic edge and hydrophilic face, which had distinct surface activity and wettability. The process involved two steps, hydrolysis and polymerization (**Fig. 9**). Firstly, the silanols of the hectorite reacted with

siloxo groups of dimethylethoxysilane (DMES), hence grafting of Si-H onto the edge of hectorite nanoparticles. Secondly, through the reaction between new created Si-H bond on the edge of grafted-hectorite and 1-octadecene, the hydrophobic alkane chains then grafted successfully onto the hectorite nanoparticle.

Fig.9.

Some organic species also can be grafted on both the external surface and internal surface of hectorite. The basal spacing of 2-(3-(2-aminoethylthio) propylthio)ethanamine (AEPE) modified hectorite increased to 18.4 Å from 12.7 Å of hectorite (Phothitontimongkol et al., 2009). A large *d* spacing of 20.1 Å was also observed after the intercalation and grafting of (3-aminopropyl)-triethoxysilane to hectorite. The grafting process consists of the condensation of ethoxy groups of (3-aminopropyl)-triethoxysilane on the surface of hectorite. With the presence of thioether group in the ligand, the van der Waals interaction among ligand chains may occur, leading to its structural rearrangement and the contraction of the interlayer spacing of hectorite.

Grafting significantly changes the physical and chemical properties of hectorite surface (Guerra et al., 2009). By a condensation reaction of the hectorite edge silanol groups with different silylating agent, different covalently-functionalized hectorite nanoparticles can be obtained. For example, the basal spacing and surface area of hectorite are increased when trialkoxy silanes are used (Wheeler et al., 2005), while flat monolayer on the edge of the hectorite plates, and only minimal effect on the basal spacing and surface area are observed when monoalkoxy silanes are used (Phothitontimongkol et al., 2013). But because of their smaller particle size, monoalkoxy silane-hectorite exhibit generally better dispersion than other large alkoxy silanes-hectorite.

In addition, the texture and properties of the surface functional groups on the grafted hectorite strongly depend on the grafting route. For example, hectorite-aminosilane hybrid materials have been prepared by a reaction of hectorite with amino silanes. The aminosilane are made from a reaction of (3-chloropropyl) triethoxysilane (CIPTES) with biuret and melamine in toluene and then to it hectorite added for grafting (González et al., 2017). Alternatively, CIPTES were slowly added to the hectorite dispersion and then biuret and melamine was added and the hydrolysis was

catalyzed by HCl acid. The toluene non-aqueous condition and the aqueous acidic condition lead to physico-chemical and adsorptive properties of the hybrids. Due to acid-catalyzed hydrolysis of the alkoxide, the hybrid made under aqueous acidic condition possessed higher specific surface area.

Due to the distinct ratio of edge to surface of 0.07 (Delavernhe et al., 2018), hectorite is used as an ideal material for studying combined edge and surface modification. Dual modification of hectorite refers to simultaneous surface modification and edge modification. In an earlier study, dual-functional hectorite was synthesized by a condensation reaction with silane coupling agents and a cation exchange reaction with quaternary ammonium cations (Wang et al., 2007). In this way, quaternary ammonium chains can be grafted to hectorite edges, creating star-like or fringed products with a nanosized inorganic core. In another study, double-chain surfactant dimethyldioctadecylammonium cation was employed as cation exchanger and 3-(trimethoxysilyl)propyl methacrylate was employed as an edge covalent modifier (Borsacchi et al., 2007). After such modification, the adjacent hectorite nanoparticles were twisted, resulting in an increased disorder in the hectorite nanoparticles. Mishra et al. (2011) prepared two types of dual modified hectorite. One was hectorite modified by cetyl trimethyl ammonium cations followed by silylation with octyl trimethoxy silane; the other was hectorite modified by cetyl trimethyl ammonium cations followed by silylation with 3-aminopropyl triethoxy silane (**Fig.10**). Then after the dual modified hectorite reacted with the hard segments of thermoplastic polyurethane (TPU), the resultant nanocomposites exhibited different aggregated morphologies (tubular, elliptical and spherical), thus resulting in the difference in segmental relaxation, and mechanical and rheological properties of the nanocomposites.

Fig.10.

4 Assembly

4.1. Layer-by-layer assembly

Layer-by-layer (LBL) assembly is a process to produce multilayered films from lamellar material by repeated assembly of one layer over the other layer. It can be conducted on polymer surface (Wagner, 2007). LBL assembly can be driven by electrostatic forces (Such et al., 2006), covalent bonds (Buck et al., 2007) or hydrogen bonding (Gao et al., 2018). Hectorite can be easily dispersed and exfoliated in water to form individual nanolayers, and by LBL technique, the nanolayers can be used to produce homogeneous and continuous hybrid film (Fenero et al., 2017).

Hectorite nanoparticles can be deposited in a LBL way and assembled on polyvinyl alcohol (PVA) surface to form films through hydrogen bonding and adsorption (Patro and Wagner, 2011). The LBL films exhibit better mechanical properties than pure PVA, mainly because hectorite nanoparticles being oriented, leading to efficient interfacial stress transfer. In addition, the overlapping dispersed hectorite nanolayers can act as individual barriers to gas infiltration and created a more tortuous and longer path for gas molecules moving through the polymer matrix (Keeling et al., 2012). Thus the transport of molecules, atoms and ions in the film can be tuned. A recent study (Patro and Wagner, 2016) revealed that graphene oxide (GO) can be dispersed in aqueous hectorite dispersion and the two nanolayers can be used for layer-by-layer assembly. In this way, GO was easily incorporated into polyvinyl alcohol (PVA)/hectorite LBL films. The LBL films appear to be uniform and the thickness of the layer increased linearly with the number of depositions.

By LBL assembly, hectorite nanolayers can be used for making multilayer reverse osmosis membranes. Generally, the multilayer reverse osmosis membrane shows excellent rejection capability, wide pH tolerance, low permeability and poor chlorine stability (Priolo et al., 2013; Liu et al., 2014b; Cho et al., 2015). The combination of the nanochannels in the interlayer of hectorite and the high porosity of the nanofiber mat support high separation efficiency with simultaneously high permeability of thin film nanocomposite nanofiber membrane. Rajeshwe et al. (2017) incorporated hectorite nanoparticles into the layers formed between trimesoyl chloride (TMC) and

m-phenylenediamine (MPD). Hectorite nanoparticles were physically attached with the amide linkages through hydrogen bonding to form the trilayer structure. The incorporation of hectorite facilitated rapid growth of the selective layer, 29 nm per layer for the trilayered TMC/MPD/hectorite, compared with 9 nm per layer of the bilayered TMC/MPD.

LBL assembly can also applied to make hectorite nanohybrids. For example, by LBL assembly Xiao et al. (2016) prepared polyelectrolyte multilayer-coated doxorubicin (DOX)/hectorite nanohybrids. DOX was firstly loaded onto the surface of hectorite via electrostatic interaction. Then DOX-loaded hectorite was alternatively coated with positively charged poly(allylamine) hydrochloride (PAH) and negatively charged poly(sodium styrene) sulfonate (PSS). The nanohybrids can be used as novel DOX delivery systems with sustainable and controllable drug release. Recently, a kind of nitrogen-doped carbon nanodot (NCND)-hectorite hybrids was obtained by LBL assembly (Dimos et al., 2017). The NCND had excellent solubility in water and abundant nitrogen-and oxygen-bearing functional groups on their surface. Hence, such small fluorescent NCND can be intercalated into the interlayer space of hectorite by an ion-exchange reaction. Firstly, dimethyldioctadecylammonium (DODA)-hectorite monolayer was prepared at the air/water interface and attached onto a substrate. Then the DODA-hectorite layer was dipped into a solution of NCND for self-assembly, resulting in a luminescent DODA-hectorite-NCND multilayer film (**Fig. 11**). Moreover, the inert hectorite nanoparticles not only guide the highly ordered 2D assembly of NCND in the interlayer space of hectorite but also protect them from external agents.

Fig.11.

4.2. Templated assembly

Hectorite nanoparticles can be assembled in a structure-oriented way with the aid of a template. Such templated assembly method can combine with LBL assembly and such methodology can be used to fabricate nano- or microcapsules with hectorite in the structure. For example, by using Pickering emulsion template and electrostatic LBL self-assembly, Liu et al. (2014a) successfully prepared nanocomposite polysaccharide microcapsules composed of

biocompatible polyelectrolyte complexes. The LBL deposition occurred between sodium alginate (ALG) and chitosan (CS) on Pickering emulsion droplets. They were stabilized by poly(ethyleneimine) (PEI) -modified hectorite nanoparticles. Hollow multilayer microcapsules are obtained after removing the core by washing with 2-propanol (**Fig. 12**). These hollow microcapsules are well-dispersed in organic solvent and show long-term stability for more than two months. In addition, the size of the microcapsules can be tuned (from several to tens of micrometers) by altering the mass ratio of PEI/hectorite.

Fig.12.

By a templated self-assembly process, a water-dispersible multifunctional polyaniline-hectorite-keggin iron nanotube has been achieved (Sudha et al., 2011). The negative ions on the surface and residual positive charges on the edges of the hectorite disc adsorbed both keggin iron and aniline through ion-dipole and ionic interactions. That is to say, hectorite can act as a micellar template during polymerisation. During polymerization, the disorganized keggin iron-hectorite nanoparticles were co-structured, and then self-assembled with the polyaniline and the engulfed layers and rolled sheets of nanotubes. The multifunctional polyaniline-Laponite-keggin iron nanotubes exhibited electrical conductivity, saturation magnetization and thermal stability (573K). More recently, Huang et al. (2018) demonstrated a co-assembly method for making ordered inverse opal-like porous hectorite films with well-defined pore size that are crack-free over a large area (on the scale of cm^2). Hectorite nanolayers were co-assembled with polystyrene latex nanoparticles into colloidal crystals. The polystyrene latex were used as a sacrificial template, which was burnt by calcination (**Fig. 13**). The change of the ratio of hectorite to polystyrene changes in the quality of film. The hygroscopic nature of the hectorite can slow the film drying and therefore mitigate cracking. Another possible reason was that the stacking and overlap of hectorite nanolayers distributed evenly the stress, thereby reducing cracking.

Fig. 13.

Janus nanoparticles are a type of nanomaterials with asymmetric structure, Namely, the two sides of a Janus nanoparticle are different in composition or polarity. The exchanging ions will change the surface charge potential of hectorite, depending on the type of ions exchanged. A hectorite nanoparticle has anisotropic surface potentials on either side and thus it can be made into Janus particles. For example, Janus colloids composed of hectorite-armored poly(divinylbenzene) can be obtained through a double Pickering emulsion template (Pardhy and Budhlall, 2010). Polystyrene or poly(divinylbenzene) colloids stabilized with hectorite were synthesized first to form hectorite-armored colloids (**Fig. 14a and b**). Then, the nanoparticle-stabilized colloids were templated at a wax-water interface in order to modify one hemisphere of the colloids (**Fig. 14c**). The hectorite nanoparticles on the aqueous side are ion exchanged (Na^+ by Ca^{2+} , Fe^{2+} , and Fe^{3+}) in the dispersion. After breaking Pickering emulsion, Janus colloids were obtained (**Fig. 14d**). The diameter of the polystyrene (PS) particle can be controlled by adjusting the ratio of oil and hectorite. Liu et al. (2013) described the assembly of amphiphilic Janus hectorite nanoparticles by using surface immobilization. The positively charged PS colloidal nanoparticles acted as templates. One side of a hectorite nanoparticle touched the surface of PS colloidal particle, and the other side of hectorite nanoparticle faced the aqueous medium (**Fig. 15**). After redispersing the colloidal PS nanoparticles into tetrahydrofuran (THF)-water mixture, amphiphilic Janus hectorite nanolayers with PS chains on one side and hydrophilic quaternized poly(2-(dimethylamino)ethyl methacrylate(q-PDMAEMA) or polymeric micelles on the other side were obtained.

Fig. 14.

Fig. 15.

4.3. Hierarchical assembly

Supramolecular self-assembly based on multiple noncovalent forces is an effective way to fabricate multiple stimuli-responsive hydrogel. However, such organic supramolecular

nanstructured materials are always subjected to weak mechanical strength. The hierarchical organic-inorganic supramolecular assembly can introduce hectorite into the supramolecular hydrogels and enhance the mechanical properties of supramolecular hydrogels. It also reduces the organic consumption. Supramolecular hydrogel with strong luminescence, extraordinary mechanical property, and self-healing ability were also obtained by hierarchical organic-inorganic self-assembly (Li et al., 2017a; Li et al., 2017b; Li et al., 2018). An organic ligand consisting of a terpyridine unit and two flexibly linked methylimidazole moieties (**Fig. 16a**) acted as emitting sources (Li et al., 2017a). Synergistic coordination of thenoyltrifluoroacetone and terpyridine units led the monomer to self-assemble into spherical micelles in water, thus maintaining the luminescence of Ln complexes in water (**Fig. 16b**). These micelles further co-assemble with sodium polyacrylate (ASAP)-exfoliated hectorite nanolayers into networks (**Fig. 16c**). Association of hectorite nanoparticles coated with oxanions with the imidazolium salts on the surface of the supramolecular assemblies via electrostatic interactions resulted in formation of robust luminescent hydrogels. Another design proposed the self-supported supramolecular hydrogels can be constructed through the hierarchically assembly of hectorite with cyclodextrin-based pseudopolyrotaxanes (PPRs) (Li et al., 2017b). The cooperative interactions between the PPR-involved guanidinium parts and the negatively charged hectorite nanoparticles played a crucial role in the formation of supramolecular hydrogels. The hydrogels have tunable mechanical strength, which modulated by tuning the molecular weight of polymeric chains in the central pseudopolyrotaxanes. Later, Ln ions and guanidinium-azobenzene (Guazo) units were chose as luminescent emitting ions and photo-switches (Li et al., 2018). The host-guest complexes consist of α -cyclodextrins (α -CDs) and azobenzene (**Fig. 17**). The Ln-containing host-guest complexes subsequently served as binders for the incorporation of exfoliated hectorite into the hydrogels. The hybrid luminescent hydrogels were formed through the construction of multivalent salt bridges involving hydrogen bonding and electrostatic interactions between the guanidinium groups and the oxanion groups on the surface of the hectorite. These luminescent supramolecular hydrogels showed excellent mechanical strength, color-tunable luminescence, and photoirradiation reversibility.

Fig.16.

Fig.17.

Besides, two types of nanoparticles of clay minerals can be mixed together to be added into hydrogels. Hectorite (aspect ratio of 25) and montmorillonite (aspect ratio of 250) were used to fabricate bicontinuous gels by hierarchical self-assembly (Pujala et al., 2018). The bicontinuous gels exhibited foam-like morphology with pore size of a few micrometers. The pore size in bicontinuous gels can be tuned by varying the g ratio of hectorite/montmorillonite nanoparticles (Fig. 18).

Fig. 18.

5. Applications

Hectorite has been commercially used in such industries as cosmetics, detergents, coatings, and paints in which the excellent colloidal properties of hectorite nanoparticles are advantageous. A small amount of hectorite is added into the polymeric system can form functional hydrogels with improved properties. Hectorite can also be used as adsorbents and catalysts. Recent years has witnessed that hectorite nanoparticles are increasingly studied for being used in analysis, energy materials and biomaterials. For instance, hectorite-coated spherical silica particles were used as chiral high performance liquid chromatography column packing materials (Tomohiko et al., 2018). The layered hectorite nanoparticles can improve optical resolution and reduce the volume of mobile phase used. Yang and Zhang (2018) successfully developed a hectorite nanolayer/carbon black-coated Celgard separator to inhibit polysulfide shuttle of lithium-sulfur (Li-S) battery efficiently. Besides, the abundant Li^+ and the layered nanostructure of the hectorite nanolayer enhanced the Li^+ conductivity. Consequently, the Li-S batteries showed a high initial reversible capacity, high rate performance, superior cycling stability, and ultralow self-discharge.

5.1. Adsorbent

Hectorite has been used as adsorbents for selectively adsorbing heavy metals, gas, dye and organic compounds. The driving force of adsorption involves chemical bonding, electrostatic attraction, Van der Waals force, surface complexation, and ion exchange between adsorbates and the surface of hectorite. In addition to surface reactivity, the adsorption behavior of hectorite is also related to the oxygen defects of the Mg–O octahedra and the Si–O tetrahedra (Bian et al., 2015).

Some studies suggested that hectorite has better adsorption selectivity and capacity towards metal ions after being modified with organic ligands-containing metal-chelating groups. For example, 2-(3-(2-aminoethylthio) propylthio) ethanamine (AEPE)-modified hectorite is a good adsorbent for Hg(II) ions with adsorption capacity of 54.7 mg/g in a solution contained 140 mg/l Hg(II) ions at pH 4 (Phothitontimongkol et al., 2009). AEPE-hectorite also showed a good selectivity toward silver ions in the solution pH ranged from 4 to 9 and the maximum adsorption capacity was 49.5 mg /g (Phothitontimongkol et al., 2013). The improvement is ascribed to high affinity of the AEPE ligand for binding Ag(I) ions and Hg(II) ions, preventing the detachment of the metal ions from the surface of hectorite. Similarly, the adsorption capacity of bis[3-(triethoxysilyl)propyl] tetrasulfide-modified hectorite for U(VI) from wastewater (18.99 mmol/g) comes from the high affinity for binding silver ions of the ligand (Guerra et al., 2010; Lee and Koo, 2011)

Pillared hectorite also has selective adsorption for gas because of the high specific surface, the size and volume of micropores, and of the pillars. Pillared hectorite showed an adsorption selectivity for CO₂ over N₂, and the volume ratio of adsorbed CO₂ to adsorbed N₂ reached 1.9 at 303K (Pawar et al., 2009). The mesoporous hectorite based on calcined tetraphenylphosphonium-modified hectorite had a high surface area of 384 m²/g and showed a very good adsorption selectivity for CO₂ over N₂, CO, CH₄ and O₂ (Sethia et al., 2014). The CO₂ adsorption capacity for mesoporous hectorite was 22.8 cm³ /g at 288 K. Theoretically, CO₂ has higher quadrupole moments and polarizability than N₂, CO, CH₄ and O₂. The principal interaction of the gas molecules with hectorite came from the electrostatic interaction between lattice oxygen

atoms and interlayer Li^+ cations of hectorite, and this electrostatic interaction depends on the quadrupole moments, dipole moment and polarizability of the gas molecules.

Dyes in the wastewater cause environmental issues because they are toxic, mutagenic or carcinogenic. Hectorite has been experimentally used as an adsorbent for the removal of cationic dyes. The interaction between hectorite and cationic dyes were divided into two ways, ion exchange (Baskaralingam et al., 2007; Fujimura et al., 2016) and electrostatic interactions (Lezhnina et al., 2012). For example, cetylpyridinium-modified hectorite acted as an effective adsorbent for Neutral Red in aqueous solution and showed an adsorption capacity of 393.70 mg/g (Yue et al., 2011). The adsorption capacity of hectorite for methylene blue (MB) at pH 6.5 was 1.162 mmol/g (Hegyesi et al., 2017). In this case, the isoelectric point at the edge and the negatively charged basal surface of hectorite were covered by MB^+ cations (Pawar et al., 2018).

Hectorite is also used to adsorb organic compounds. Aflatoxin, a kind of toxic and carcinogenic biotoxin, can be adsorbed by hectorite (Bbosa et al., 2013). The diffused octahedral layer charge in hectorite allowed more accessibility to the interlayer space and less repulsion for aflatoxin molecules than other smectites where the charge was of tetrahedral origin. In addition, the size and polarity matching between the adsorbing domains and aflatoxin molecules in the interlayer was influenced by the exchangeable cation (Barrientos-Velázquez et al., 2016). Trimethoprim, 5-(3,4,5-trimethoxybenzyl) pyrimidine-2,4-diamine (TMP), is an antibiotic drug that cannot be completely metabolized by the human being (Ji et al., 2016). When the hectorite was grafted with aminosilane, the presence of well-dispersed active sites favors the adsorption of TMP onto hectorite-aminosilane hybrid materials. The interactions between trimethoprim and hectorite are hydrogen bonding and Lewis acid-base interactions and cation exchange. As a result, the removal percentage for TMP was larger than 80% (González et al., 2017).

5.2. Catalyst

Hectorite have been widely used as a host or a support for metal-based catalysts and oxide-based catalysts. Incorporating the active metals (e.g. Ru, Cu) or oxides into the interlayer space of hectorite allows those active species to be highly dispersed, thus enhancing acid-base or redox catalytic performance. So far the catalytic properties of hectorite have been experimentally

evaluated for many catalytic reactions (**Table 3**). Generally, due to the thermal stability of hectorite, the temperatures for the catalytic reactions upon heating are not as high as 873K.

Cu can be supported onto delaminated hectorite by impregnation and ion-exchange methods. The Cu/hectorite catalyst has proved catalytically active for the selective glycerol hydrogenolysis to 1,2-propanediol in liquid phase (Sánchez et al., 2012). The conversion of glycerol can reach to 61% and the selectivity to 1,2-propanediol was 93% after 8 h of reaction at moderate conditions (40 bar, 473 K). The high surface area and lower hydrophilic character of the delaminated hectorite played a role in avoiding Cu agglomeration. Cu/delaminated hectorite catalyst was also able to accelerate the oxidation of NO to NO₂ (Sánchez et al., 2013a). For a gas mixture of 500 ppm NO_x/5% O₂/N₂, over the Cu/hectorite catalysts for 5000s at 873K, the soot conversion can reach 100%. The main role of the Cu/hectorite catalyst was to activate O₂ molecules, thereby facilitating NO to NO₂. Hectorite can also be introduced into the microgel of cationic Pb precursors by ion exchange to obtain Pd-containing ternary microgel nanocomposites. The microgel nanocomposites as catalysts are active for the Suzuki reaction of aryl iodides in water-rich medium under mild condition (353K, 4h). The higher catalytic efficiency was observed in the case of microgels with the higher hectorite content (Contin et al., 2014).

Ru nanoparticles can be intercalated in the interlayer space of hectorite to give a black solid catalyst (Süss-Fink et al., 2006). The Ru nanoparticles/hectorite exhibited hexagonal or spherical shapes with the size in the range of 4–38 nm. It was a highly efficient and reusable catalyst in the hydrogenation of benzene (Süss-Fink et al., 2009). Ru/hectorite nanoparticles can catalyze the hydrogenation of benzene to cyclohexane under mild conditions (323K) and the turnover frequencies (TOF) reached up to 6500 catalytic cycles per hour (Süss-Fink et al., 2009). Ru/hectorite nanoparticles (particle size ~ 4nm) were also able to catalyze the hydrogenation of furfuryl alcohol to tetrahydrofurfuryl alcohol in methanolic solution at 313K under a hydrogen pressure of 20 bar (conversion 100%, selectivity>99%) (Khan et al., 2011). After a total turnover number of 1423, Ru/hectorite nanoparticles were deactivated but can be recycled and regenerated. In addition, Ru/hectorite (particle size ~7 nm) was found to catalyze the specific hydrogenation of the C=C bond in α,β -unsaturated ketones (conversion 100%, selectivity > 99.9%) (Khan et al., 2012). The catalytic turnovers range from 765 to 91,800 under mild conditions (temperature 308K

and constant hydrogen pressure 1–10 bar). Besides, Ru/hectorite nanoparticles can also catalyze the hydrogenation of quinoline at 373K under 30–60 bar H₂ with solvent-switched selectivity: in water, 1,2,3,4-tetrahydroquinoline was formed with yields >99%, whereas in cyclohexane the fully hydrogenated decahydroquinoline was obtained with yields >99% (Sun et al., 2013).

FeO_x-pillared hectorite was a highly effective catalyst for the conversion of epoxides to acetanilides (Trikittiwong et al., 2014). The preparation of catalyst mainly involved the intercalation of FeCl₃ into hectorite interlayers and calcination. At 303K for 30min, the conversion of styrene oxide to 2,2-dimethyl-4-phenyl-1,3-dioxolane by different FeO_x-pillared hectorite catalyst in 83% yield. In addition, the catalyst can be recovered and reused up to five times without appreciable loss of activity. More recently, researchers have been discovered that the adsorption of the amino acid on the surface of hectorite led to the increased enantioselectivity in the asymmetric Michael addition (Szöllősi et al., 2018). The heterogeneous chiral catalyst maintained stereo selectivity in the asymmetric addition of aldehydes to nitrostyrenes.

A class of thermally stable and mesoporous metal oxide/ hectorite nanoparticles have been earlier studied by Zhu et al (2002, 2006) for the degradation of Rhodamine 6G in aqueous solution. TiO₂/hectorite proved to be a heterogeneous photocatalyst (Hashimoto et al., 2005). In particular, mesoporous TiO₂/hectorite had large mesopores which were beneficial to the diffusion of organic molecules to access to the active sites (Yang et al., (2010). The use of hectorite could help to form a specific TiO₂ nanoparticles with high photocatalytic activity. Recently, a photocatalytic hybrid film of anatase and hectorite was successfully fabricated by Deepracha et al. (2019). The film was adhered on the glass substrate stably enough for the photocatalytic decomposition of methylene blue and methyl orange in an aqueous acidic solution.

Hectorite have also been used for the controlled formation and stabilization of core-shell nanocrystals with enhanced stability and large surface area. This core-shell Pd–Pt-hectorite composites were active catalysts for the reduction of 4-nitrophenol with NaBH₄ in aqueous solution (Varade and Haraguchi, 2014). As a result of the presence of hectorite, the catalysts showed superior resistance to undesirable agglomeration of active sites and thus exhibited the exceptional catalytic activity. Bis(oxazoline)-metal complexes have been used as catalysts in many enantioselective reactions. They can be supported by cationic exchange into hectorite, and

that the solids thus obtained are able to promote the benchmark cyclopropanation reaction between styrene and ethyl diazoacetate with the enantio selectivity in the range of 16-20% (Ben Zid et al., 2017).

Table 3

5.3. Fluorescent reporter

Hectorite can act as a carrier for many organic dye molecules for functionality in optical spectroscopic analysis. Typically, dye/hectorite hybrid nanomaterials combine the optical and spectroscopic properties of organic dyes with the physical and chemical properties of hectorite (Duque-Redondo et al., 2014). The hybrid nanomaterials have a potential for nanoscale fluorescent reporters and optical probes for a variety of fluorescence-based analytical and diagnostic applications (Suzuki et al., 2011; Dawson and Oreffo, 2013; Takagi et al., 2013; Elder et al., 2014; Fujimura et al., 2016).

The adsorption of organic fluorophores such as methylene blue (Schoonheydt, 1991), toluidine blue (Yurekli et al., 2005), rhodamine 6G (R6G) (Arbeloa and Martínez, 2011) and crystal violet (Ley et al., 2015b) onto the hectorite surface is mainly driven by electrostatic interactions. Generally, dispersing the dye on the hectorite surface enriches dye population and (Yurekli et al., 2005). Fluorescence polarization is used for evaluating the preferential orientation of fluorescent dyes adsorbed in hectorite layers in a macroscopic scale (Arbeloa and Martínez, 2011). For example, R6G monomers were adsorbed onto the hectorite layers as monomeric units for low-loading films, with a preferential orientation of around 62° with respect to the normal of the film. Indeed, the electrostatic interactions between negatively charged basal surface of hectorite nanoparticles and dye molecules can be used to tune the photophysical properties of dye. Ley et al. (2015b) found that the strong electrostatic interaction between hectorite and Crystal Violet cationic molecules hinders phenyl ring movements and consequently inhibited the formation of dark state. As a consequence, light energy was stored in a singlet emissive bright state, turning this nonemissive dye into a fluorescent one. Similarly, the electrostatic interaction of

Astrazon orange R (AO-R) on the hectorite nanoparticles prevented the isomerization of the dye after light absorption, stabilizing the emissive singlet excited state of the dye (Tsukamoto et al., 2015; Ley et al., 2015a).

Hectorite has been experimentally loaded with perylenes, cyanines, merocyanines, and coumarines (Grabolle et al., 2016). The adsorption of such neutral dyes or zwitterionic dyes onto the hectorite was achieved by van der Waals interactions (Suzuki et al., 2011) and hydrogen bonding (Dawson and Oreffo, 2013). Adsorption of the dyes onto hectorite nanolayers brought about changes in the spectra and intensity of absorption and emission. The intensity was dye-specific, depending on dye charge and character of the optical transitions involved. The fluorescence quantum yields reached at least 0.20 even at the highest dye loading concentration of up to 50 dye molecules per hectorite platelet. This was because hectorite had flat surface at atomic level, positive or negative charges in the structure and optical transparency in a state of aqueous dispersion. Dye molecules on the hectorite surface could change their structure and intramolecular vibrational motion, thus changing their fluorescence properties (Tokieda et al., 2017). This fluorescence enhancement phenomena of dyes on the hectorite surface are named as “Surface-Fixation Induced Emission (S-FIE)”.

The loading of hydrophobic dyes onto hectorite makes it accessible in aqueous environments (Gaharwar et al., 2013). Besides, combining different types of organic dyes and hectorite can tailor photoactive properties (Staniford et al., 2015) and the microscopic order of the dye molecules and make them homogeneous dispersed (Hill et al., 2015). For example, employing hectorite as inorganic matrix combined with native aluminium hydroxide phthalocyanine (Al(OH)Pc) led to a novel organic–inorganic hybrid materials (Staniford et al., 2015) (**Fig. 19**). Not only were the solubility and aggregation bottleneck of Al(OH)Pc tackled simultaneously, but also the efficient emission of Al(OH)Pc–nanoclay hybrids and generation of singlet oxygen was achieved in aqueous solution.

Fig. 19.

Dye/hectorite hybrid nanomaterials can act as nanoscale fluorescent reporters for fluorescence-based analytical and diagnostic applications. For example, hectorite-Astrazon orange R(AO-R) can form very efficient hybrid photoinitiators. The dye molecules were intercalated in the interlayer space, located at the edges or at the surfaces of the stacked layers. Hence, the photophysics of the AO-R molecules can be adjusted. The conversion rates at a constant resin viscosity were increased by the 4-fold (Ley et al., 2017). Li et al. (2015) demonstrated an organic-inorganic nanohybrid luminescent pH detector by loading a Europium(III) - β -diketonate complex into hectorite. It worked under acid conditions and can serve as highly robust, reliable, rapid responsive and sensitive fluorescent pH detector. Au/hectorite nanoparticles as enhanced substrates can be applied to surface enhanced Raman scattering (SERS) (Hill et al., 2016). Hectorite not only played the role of template during the growth of Au nanoparticles, but also increased dye adsorption, thus achieved the enhanced local electric fields generated by the plasmon, thus improving the SERS sensitivity.

In addition, the presence of hectorite nanoparticles in the solution not only influences the optical properties of the dye, but also influences other properties. The aggregation of cationic p-phenylene ethynylenes oligomers (OPE) exhibited strong antimicrobial activity and strong photophysical changes, can thus be utilized for sensing various chemicals and biomolecules (Tang et al., 2011). OPE aggregate on hectorite and induce aggregation of hectorite nanoparticles, leading to drastic changes to their photophysical properties and other properties. Solid OPE-hectorite films were shown to have fair resistance to dissolution in aqueous solution compared with hectorite alone (Hill et al., 2015). Besides, in presence of hectorite, the second harmonic generation (SHG, also called frequency doubling) active J-aggregate of a thiacyanine dye N, N'-dioctadecylthiacyanine perchlorate (TC18) in Langmuir-Blodgett (LB) films exhibited good stability due to the presence of electrostatic force between thiacyanine dye and hectorite (Debnath et al., 2017).

5.4. Hydrogel

Hydrogel is a large water-filled inorganic or organic polymeric network in variable gel form. Hydrogels are mainly formed via physical or chemical crosslinking of inorganic or organic

molecules or nanoparticles. Usually, physical hydrogels are unstable while chemical hydrogels are brittle and lacking of self-healing ability (Raeburn et al., 2013; Zhao et al., 2015). Supramolecular self-assemblies based on multiple noncovalent forces have emerged as an effective way to fabricate multiple stimuli-responsive and self-healable intelligent hydrogels. Hectorite nanoparticles and polymer can synergistically work together to produce a supramolecular hydrogel with improved biological, chemical, mechanical and physical properties. In particular, recent studies have indicated that such inorganic-organic hydrogels provide a biomimetic and hydrated 3D microenvironment (Annabi et al., 2014; Pedron, et al., 2015; Ma et al., 2018).

Hectorite nanoparticles form delaminated dispersions in water and self-assemble via face-edge aggregation, creating an open, macroporous and thixotropic hydrogel network (Takahashi et al., 2005). Nevertheless, hectorite nanoparticles is often used to improve the mechanical properties of a supramolecular hydrogel. For example, Wang et al. (2010) reported a kind of supramolecular nanocomposite hydrogel with high mechanical strength and a fast-recovery capability. The hydrogel consisted of four components: water, hectorite nanolayers, a dendritic macromolecule (Gn-binder) and sodium polyacrylate. The hydrogelation occurred by kinetic trapping of the 3D network structure formed by the adhesion of G3-binder onto hectorite nanolayers. The improved mechanical strength resulted largely from the mechanical toughness of hectorite nanolayers. The hydrogel of poly(N-isopropylacrylamide) (PNIPAM) and hectorite with a nacre-like brick-and mortar arrangement of organic and inorganic layers showed enhanced mechanical properties and transparency (Wang et al., 2012). The noncovalent interactions between hectorite and PNIPAM were hydrogen bonding between amide side groups (-CONH) on PNIPAM and the surface SiOH or Si-O groups of the hectorite. The excellent mechanical properties were attributed to the layered micro-/ nanoscale structure and the unique polymer/hectorite network.

Hectorite nanoparticles not only increased the strength of the hydrogel but also impacted the toughness of the hydrogel. Organic-inorganic hybrid self-assemblies can not only enhance the mechanical but also change optical properties of supramolecular hydrogels. Li et al. (2017a; 2017b; 2018) constructed self-supported supramolecular hydrogels through the hierarchically organic-inorganic hybridization of hectorite matrix with organic ligands. The cooperative interactions between the organic ligand parts and the negatively charged hectorite nanolayers

mainly contributed to connection of the organic and inorganic components to form the supramolecular hydrogels. The luminescent supramolecular hydrogels consist of emitting sources, organic ligand and hectorite are transparent, have self-healing properties and tunable mechanical strength (Li et al., 2017a). Multifunctional nanocomposite gels consisting hectorite, isocyanate (NCO)-terminated sP(EO-stat-PO) macromers, and clickable bicyclononynes (BCN) are biocompatible, slowly degradable, and possess high mechanical strength (Topuz et al., 2017). Even though the NCO-sP(EO-stat-PO) macromers could form a hydrogel network in water, the incorporation of hectorite led to significant improvement of the mechanical properties.

Hydrogels have great potential for 3D printing. Remarkably, they can be rapidly printed into complex 3D structures for cell culturing and tissue engineering (Kolesky et al., 2014). Hectorite nanoparticles have been experimentally mixed with various responsive hydrogel precursors to improve their 3D printability. Hong et al. (2015a) prepared the polyethylene glycol (PEG)-alginate-hectorite hydrogels as the ink of a 3D printer. Hectorite significantly enhanced the viscosity of PEG-alginate hydrogel and increased its shear-thinning properties. The hydrogels can be printed into diverse shapes and suitable for long-term human mesenchymal stem cells (hMSC) culture. More recently, hectorite was found to be an effective additive to improve the self-supporting printability of N-isopropylacrylamide (NIPAAm), a thermoresponsive hydrogel precursor (Jin et al., 2018). Therein graphene oxide (GO) was further added to respond to near-infrared radiation and thus worked as a nanoscale heater (**Fig. 20**). Hectorite can be mixed with these responsive hydrogel precursors of NIPAAm to improve their 3D printability. The methodology pNIPAAm-hectorite-GO nanocomposite hydrogels can be further applied to prepare various 3D printable responsive nanocomposite hydrogels.

Fig. 20.

Deoxyribonucleic acid (DNA) hydrogels are water-swollen 3D networks of DNA strands. DNA hydrogels have such unique properties as biocompatibility, highly selective binding, and molecular recognition. Nevertheless, DNA hydrogels suffer from poor mechanical properties and low dimensional stability (Okay, 2011). Introducing hectorite into DNA hydrogels improves the

stability of DNA hydrogels due to the strong electrostatic interactions between DNA molecules and the positively charged edges of hectorite (Arfin and Bohidar, 2013). Interconnecting linear poly(N-isopropylacrylamide) chains, double-stranded(ds)-DNA strands, and hectorite nanoparticles can form a 3D network of hydrogels (Uzumcu et al., 2016). Hectorite nanoparticles acted as a multifunctional dynamic cross-linkers, and the non-covalent interactions made the strong DNA hydrogels sensitivity to temperature. Uzumcu et al. (2018) recently prepared by in situ polymerization of N,N-dimethylacrylamide (DMAA) in aqueous solution of double-stranded(ds)-DNA (2-8 w/v %) in the presence of hectorite nanoparticles. The DNA/hectorite hydrogel had high stretchability (up to 1500%) and a tensile strength between 20 and 150 kPa. Hectorite nanoparticles acted as a chemical cross-linker and promoted the elastic behavior of the hydrogels, whereas DNA contributed to their viscoelastic energy dissipation.

5.5. Biomedical materials

Hectorite has great potential for drug vehicle, regenerative medicine and tissue engineering (Hoppe et al., 2011). The swellability, delamination and the structure of “house-of-cards” of hectorite makes it possible to host many biological and medical compounds. In particular, hectorite hydrogels allows a one-step procedure for the encapsulation and delivery of drugs and there is no need for tedious and costly chemical/physical process (Dawson et al., 2011). In addition, hectorite nanolayers offers efficient affinities for protein-based antigen molecules via electrostatic force (Dawson et al., 2011). Moreover, hectorite finally degrades into Na^+ , Mg^{2+} , Si(OH)_4 , Li^+ in aqueous solution (Wang et al., 2013). The ions are non-toxic to cell (Min et al., 2014). For example, shear-thinning nanocomposite hydrogels of hectorite-gelatin were biocompatible and biodegradable (Gaharwar et al., 2014). Once hectorite nanoparticles are taken up by macrophage cells in the injection site, they may undergo biodegradation processes in the late endosome and lysosome (Chen et al., 2016). Furthermore, the incorporation of hectorite nanoparticles into nanocomposite hydrogels enhance mechanical properties. Hence, such nanocomposite hydrogels can act better as 3D scaffolds for tissue engineering. For example, the incorporation of hectorite nanoparticles into a poly (ethylene glycol) (PEG)–alginate hydrogel

significantly enhanced the compressive and tensile properties of the biocompatible hydrogel s
(Chang et al., 2010).

Hectorite can be used to prepare magnetic resonance imaging (MRI) contrast agents by providing the colloidal stability for Fe_xO_y nanoparticles, a type of contrast agent. The nanocomposite of hectorite and Fe_2O_3 had an improved relaxivity over mono-dispersed Fe_2O_3 nanoparticles (Tzitzios et al., 2010). Ding et al. (2016) developed a facile controlled coprecipitation method to immobilized Fe_3O_4 on hectorite. The hectorite- Fe_3O_4 nanoparticles had good water-dispersibility and colloidal stability, and can be metabolized and cleared out of the body. Hectorite- Fe_3O_4 nanoparticles can not only be used as a contrast agent for magnetic resonance imaging of cancer cells *in vitro* due to the effective uptake by tumor cells, but also significantly enhanced the contrast of an xenografted tumor model.

A moldable nanocomposite hydrogel combining a mussel-inspired polymer, dopamine-modified multiarmed polyethylene glycol (PEG-D) and hectorite was recently created by Liu and Lee (2016). The interactions between polymer-bound dopamine and hectorite led to the autoxidation of dopamine and the subsequent covalent cross-linking of catechol residues (Hong et al., 2015b). The nanocomposite hydrogel acted as adhesive in biomedicine and can be used for sealing tissue surfaces with a complex and non-flat geometry. A fit-to-shape sealant on the tissue has been well made by combining dopamine-modified polyethylene glycol and hectorite, without the use of cytotoxic oxidants to develop the moldable hydrogel (Liu et al., 2017). The hydrogel transformed from a reversibly cross-linked network formed by dopamine-hectorite interfacial interactions to a covalently cross-linked network through the slow autoxidation and cross-linking of catechol moieties. The hydrogel can be remolded to different shapes. It also can be recovered from large strain deformation, and can be injected through a syringe to adhere to the convex contour of a tissue surface. With time, the hydrogel solidified to adopt the new shape and sealed defects on the tissue. Such fit-to-shape sealant has great potential for sealing tissues with non-flat geometries, such as a sutured anastomosis.

Delaminated hectorite nanoparticles form good dispersion in water and undergoes self-assembly via face-edge aggregation creating an open, macroporous and thixotropic hydrogel network (Takahashi et al., 2005). The thixotropic properties of hectorite allow the establishment of

a hydrogel network sufficiently cohesive to bridge gaps about 1cm (**Fig. 21a**). Adding pre-dispersed hectorite into electrolyte solutions generates gel capsules. The morphologies progressing from amorphous residues to discrete spherical capsules when physiological ionic strength (equivalent to 100–150 mM NaCl) is increased. Hectorite capsule formed in response to drop-wise addition to media of varying ionic strength (NaCl concentration) (**Fig. 21b**). Cells suspended in hectorite formulations of low viscosity were encapsulated by direct addition to cell culture media (**Fig. 21c**). The hectorite capsules had good cytocompatibility and can incorporate extra-cellular matrix molecules to modulate the behavior of encapsulated populations. Such hectorite capsules can stimulate angiogenesis *in vitro* and *in vivo* following a brief exposure to soluble vascular endothelial growth factor (**Fig. 21d**) (Dawson et al., 2011). The bioactive nanoparticles based on the interaction of hectorite nanoparticles with bone tissue at cellular levels was also revealed (Gaharwar et al., 2013). In the absence of any osteoinductive factor, the hectorite capsules promoted *in vitro* osteogenic differentiation of human mesenchymal stem cells (hMSCs) and such work opens a possibility to use hectorite for coating bone-recovery materials.

Fig. 21.

Hectorite has been widely used in the pharmaceutical industry both as excipients and active substances (Carretero, 2002). The high anisotropy of electrostatic interaction enabled the encapsulation of drug molecules within the interlayer space of hectorite with a high retention capacity of drug (Takahashi et al., 2005). Hectorite-protein interaction has been harnessed in drug delivery to delay or localize therapeutic molecules through hydrophobic and interlamellar mechanisms. Besides, hectorite has a remarkable capacity for protein retention because the flocculation of hectorite nanoparticles in saline solutions enhances the adsorption of active molecules (Nennemann et al., 2001). When hectorite nanoparticles are dispersed in a drug solution, it can be recovered as a drug-clay solid phase and dried so that it can be made into tablets (Aguzzi et al., 2007). In addition, hectorite can help insoluble organic compounds to distribute well in water. For example, the hybridization of itraconazole (ITA) with hectorite can enhance water solubility and facilitate controlled release (Jung et al., 2008). In other words, hectorite can be used

as a solubility controller or helper by the intercalation of organic drug molecules into the interlayer space of hectorite.

Dox is a commonly used chemotherapeutic drugs but its efficacy is limited due to its low ability for tumor tissue penetration, insufficient cellular uptake and drug resistance. Through an ion exchange reaction, Dox was encapsulated into the interlayer space of hectorite with an exceptionally high loading efficiency of $98.3 \pm 0.77\%$ (Wang et al., 2013). Hectorite/Dox complexes also can act as a promising platform for tumor therapy (Li et al., 2014). Hectorite/Dox nanohydrogel allows to release the drug in the acidic environment of the endolysosome, and helps in disrupting the endolysosome. It was biocompatible and is cleared out of body after post-treatment for 45 d. Dox can also be encapsulated within hectorite/alginate hybrid nanocarriers (Gonçalves et al., 2014). Firstly, Dox was loaded onto biocompatible anionic hectorite nanolayers through strong electrostatic interactions to get DOX-loaded hectorite nanoparticles (**Fig. 22**). Then, alginate (AG) was coated onto the Dox-loaded hectorite nanoparticles (hectorite/Dox /AG nanohybrids) to prevent the burst release of the drug. The hectorite/Dox/AG nanohybrids had high encapsulation efficiency ($80.8 \pm 10.6\%$), were sensitive to pH, and displayed a sustained drug release behavior. The biocompatibility, high loading capacity and stimulus responsive release of cationic chemotherapeutic drugs of hectorite/alginate nanohybrids, make them excellent platforms for drug delivery. Targeting agents, such as folic acid (Wu et al., 2014) or lactobionic acid (Chen et al., 2015), were conjugated on the surface of hectorite. Lactobionic acid-modified hectorite and folic acid-modified hectorite proved to be able to encapsulate Dox with an efficiency of 91.5% and $92.1 \pm 2.2\%$, respectively. The modified hectorite can specifically deliver targeting agents to tumor cells and displayed targeted inhibition efficacy.

Fig. 22.

Besides, hectorite has been used for building hybrid theranostic nanoplatfoms. Zhuang et al. (2017) invented a hectorite-PLA-PEG-PEI-(Au⁰)₅₀-HA/Dox nanocomplexes which displayed good stability, high drug loading efficiency ($91.0 \pm 1.8\%$), and sustained drug release with a

pH-sensitive manner. The combination of polyethylenimine (PEI) and hectorite takes the advantage of the ultrahigh drug loading efficiency of hectorite and the abundant amine groups on PEI for stabilizing Au NPs as computed tomography (CT) imaging contrasts and conjugating targeting agents. The nanomaterials significantly inhibit the growth of tumors and decrease the side-effect of Dox. They can also be used as a targeted contrast agent for CT imaging of tumors. More recently, Xu et al. (2018) developed a targeted therapeutic agent for photothermal and photodynamic treatment of cancer cells overexpressing integrin $\alpha\beta3$ (**Fig. 23**). Indocyanine green (ICG) was intercalated into the interlayer space of synthetic hectorite via an ion exchange reaction (**Fig. 23a**). Such encapsulation of ICG in hectorite increased the stability of ICG in solution, and the coating of polydopamine (PDA) on the surface of ICG/hectorite provided additional photothermal conversion efficacy, and facilitated the targeting modification of a nanopatform (**Fig. 23b**). Such ICG/hectorite–PDA–PEG–RGD nanoparticles showed a high encapsulation efficiency of 94.1% (**Fig. 23c**). These nanoparticles can specifically target at cancer cells overexpressing integrin $\alpha\beta3$, enhance cellular uptake and exert improved photothermal and photodynamic therapeutic effect on targeted cells upon Near Infrared(NIR) laser irradiation. In addition, Becher et al. (2018) prepared a nanohydrogel drug delivery platform consisting of hectorite nanolayers, polyacrylate, and sodium phosphate salts. The nanohydrogel was held by an outer shell of hectorite nanolayers aligned edge-to-edge probably intercalated with the polyacrylate polymer and sodium ions to balance the charges (**Fig. 24**). The guest molecules remained trapped in the tridimensional ionic hydrogel network during this process. The nanohydrogels appeared biocompatible, biodegradable, pH-responsive, and noncytotoxic. Such hydrogels are versatile platform because they e can simultaneously encapsulate several cancer drugs. Namely, they are an efficient drug cocktail delivery system and presents a positive synergistic effect.

Fig. 23.

Fig. 24.

6. Summary and remarks

Hectorite, as an easily synthesized and gel-formed clay mineral, has captured particular attention of scientists and technologists since the middle of the 20th century. An upsurge of developing strategies for modification and new applications is seen in recent decades. Despite the fact that of hydrothermal synthesis of hectorite are well commercialized, new quicker and cleaner processes, typically melt solid-state reaction and continuously microfluidic synthesis, are emerging and needed, with an objective to better achieve. quicker delamination of synthetic hectorite and higher aspect ratio of hectorite nanolayers. During the process, the extent to which hectorite delaminate, the size of hectorite nanolayers or layer charge density of the hectorite and also modification will be finely controlled simultaneously.

In addition to ion exchange, intercalation, and pillaring, many new strategies for modifying hectorite have now been developed. Surface engineering and tactic assembly of hectorite nanolayers allow many hectorite-based nanohybrids and hierarchical materials to be fabricated. Accordingly, the applications of hectorite have been significantly broaden. As well-defined 2D nanolayers, the assembly of hectorite nanoparticles with other molecules into functional films and membranes or hierarchical materials seems to be the most promising research topics. In this context, many nanoparticles and polymers have not been yet touched. Nevertheless, it should not be neglected that the conventional yet exclusively characteristics of hectorite, such as hydrogelation and thickening, rheological and thixotropic properties can be utilized in a wide range of fields and it worth further developing. Particularly, such features are essential in 3D printable ink materials and smart soft matter.

In-depth understanding of physical and chemical properties of hectorite and new modification and assembly of hectorite nanoparticles are needed. In addition to adsorbents and catalysts, increasing concerns are about the uses of hectorite for making fluorescent reporters, biosensors, drug carriers and biomaterials for cell culture, tissue engineering and tumor therapy. Nevertheless, the insights into the functionality and inherent chemical and biological mechanism of hectorite-based materials *in vivo* remain in infancy and are still elusive. With the rapid development of cleaner synthesis process technology, tactic modification and assembly, the

applications of the hectorite will be further expanded. Because synthetic hectorite possess exclusive nanostructure, nanoscale interlayer space and nanolayer, to use for surface plasmon resonance catalysts, biosensors, targeted drug vehicles, and tissue engineering materials could be new driving force to stimulate the expansion of synthetic hectorite in industry and related profitable marketplace in near future.

Acknowledgments

The authors wish to acknowledge the financial support from the National Natural Scientific Foundation of China (41672033; 21373185), the financial support by the open fund from Key Laboratory of Clay Minerals of Ministry of Land and Resources of the People's Republic of China, Engineering Research Center of Non-metallic Minerals of Zhejiang Province, Zhejiang Institute of Geology and Mineral Resource, China (ZD2018K04), and the State Key Laboratory Breeding Base of Green Chemistry-Preparation Technology, Zhejiang University of Technology (GCTKF2014006)

References

- Aguzzi, C., Cerezo, P., Viseras, C., & Caramella, C. (2007). Use of clays as drug delivery systems: possibilities and limitations. *Applied Clay Science*, 36(1): 22-36.
- Annabi, N., Tamayol, A., Uquillas, J.A., Akbari, M., Bertassoni, L.E., Cha, C., Camci-Unal, G., Dokmeci, M.R., Peppas, N.A. and Khademhosseini, A., 2014. 25th anniversary article: Rational design and applications of hydrogels in regenerative medicine. *Advanced Materials*, 26(1): 85.
- Arbeloa, F.L. and Martínez, V.M., 2011. Orientation of Adsorbed Dyes in the Interlayer Space of Clays. 2 Fluorescence Polarization of Rhodamine 6G in Laponite Films. *Chemistry of Materials*, 18(6): 393-5.
- Arfin, N. and Bohidar, H.B., 2013. Ergodic-to-nonergodic phase inversion and reentrant ergodicity transition in DNA-nanoclay dispersions. *Soft Matter*, 10(1): 149-156.

- Awad, W.H., Beyer, G., Benderly, D., Ijdo, W.L., Songtipya, P., Jimenez-Gasco, M.d.M., Manias, E. and Wilkie, C.A., 2009. Material properties of nanoclay PVC composites. *Polymer*, 50(8): 1857-1867.
- Barick, A.K. and Tripathy, D.K., 2010. Preparation and characterization of thermoplastic polyurethane/organoclay nanocomposites by melt intercalation technique: Effect of nanoclay on morphology, mechanical, thermal, and rheological properties. *Journal of Applied Polymer Science*, 117(2): 639-654.
- Barker, R.M. and Jones, D.L., 1970. Chemistry of soil minerals. Part VIII. Synthesis and properties of fluorhectorites. *Journal of the Chemical Society A Inorganic Physical Theoretical*: 1531-1537.
- Barrer, R.M. and Dicks, L.W.R., 1967. Synthetic Alkylammonium Montmorillonites and Hectorites. *Journal of the Chemical Society A Inorganic Physical Theoretical*.
- Barrientos-Velázquez, A.L., Marroquin Cardona, A., Liu, L., Phillips, T. and Deng, Y., 2016. Influence of layer charge origin and layer charge density of smectites on their aflatoxin adsorption. *Applied Clay Science*, 132-133: 281-289.
- Baskaralingam, P., Pulikesi, M., Ramamurthi, V. and Sivanesan, S., 2007. Modified hectorites and adsorption studies of a reactive dye. *Applied Clay Science*, 37(1-2): 207-214.
- Bbosa, G.S., Kitya, D., Odda, J. and Ogwalokeng, J., 2013. Aflatoxins metabolism, effects on epigenetic mechanisms and their role in carcinogenesis. *Health*, 5(10A): 14-34.
- Becher, T.B., Mendonca, M.C.P., de Farias, M.A., Portugal, R.V., de Jesus, M.B. and Ornelas, C., 2018. Soft Nanohydrogels Based on Laponite Nanodiscs: A Versatile Drug Delivery Platform for Theranostics and Drug Cocktails. *ACS Appl Mater Interfaces*, 10(26): 21891-21900.
- Ben Zid, T., Fadhli, M., Khedher, I. and Fraile, J.M., 2017. New bis(oxazoline)-vanadyl complexes, supported by electrostatic interaction in Laponite clay, as heterogeneous catalysts for asymmetric oxidation of methyl phenyl sulfide. *Microporous and Mesoporous Materials*, 239: 167-172.
- Bian, L., Song, M., Dong, F., Duan, T., Xu, J., Li, W. and Zhang, X., 2015. DFT and two-dimensional correlation analysis for evaluating the oxygen defect mechanism of low-density 4f (or 5f) elements interacting with ca-mt. *Rsc Advances*, 5(36): 28601-28610.

- Bickmore, B.R., Bosbach, D., Hochella, M.F., Charlet, L. and Rufe, E., 2001. In situ atomic force microscopy study of hectorite and nontronite dissolution: Implications for phyllosilicate edge surface structures and dissolution mechanisms. *American Mineralogist*, 86(4): 411-423.
- Borsacchi, S., Geppi, M., Ricci, L., Ruggeri, G. and Veracini, C.A., 2007. Interactions at the surface of organophilic-modified laponites: a multinuclear solid-state NMR study. *Langmuir the ACS Journal of Surfaces & Colloids*, 23(7): 3953.
- Bourlinos, A.B., And, D.D.J. and Giannelis, E.P., 2004. Clay–Organosiloxane Hybrids: A Route to Cross-Linked Clay Particles and Clay Monoliths. *Chemistry of Materials*, 16(12): 2404-2410.
- Bracco, S., Valsesia, P., Ferretti, L., Sozzani, P., Mauri, M. and Comotti, A., 2008. Spectroscopic observations of hybrid interfaces and gas storage in organo-clays. *Microporous and Mesoporous Materials*, 107(1-2): 102-107.
- Brandt, H., Bosbach, D., Panak, P.J. and Fanghänel, T., 2007. Structural incorporation of Cm(III) in trioctahedral smectite hectorite: A time-resolved laser fluorescence spectroscopy (TRLFS) study. *Geochimica Et Cosmochimica Acta*, 71(1): 145-154.
- Breen, C. and Komadel, P., 1995. Characterisation of moderately acid-treated, size-fractionated montmorillonites using IR and MAS NMR spectroscopy and thermal analysis. *Journal of Materials Chemistry*, 5(3): 469-474.
- Breu J., Seidl. W. and Stoll. A., 2003. Fehlordnung bei Smectiten in Abhängigkeit vom Zwischenschichtkation. *Zeitschrift Für Anorganische Und Allgemeine Chemie*, 629(3): 503-515.
- Buck, M.E., Zhang, J. and Lynn, D.M., 2007. Layer-by-Layer Assembly of Reactive Ultrathin Films Mediated by Click-Type Reactions of Poly(2-Alkenyl Azlactone)s. *Advanced Materials*, 19(22): 3951-3955.
- Carrado, K.A., 2000. Synthetic organo- and polymer–clays: preparation, characterization, and materials applications. *Applied Clay Science*, 17(1–2): 1-23.
- Carrado, K.A., Csencsits, R., Thiyagarajan, P., Seifert, S., Macha, S.M. and Harwood, J.S., 2002. Crystallization and textural porosity of synthetic clay minerals. *Journal of Materials Chemistry*, 12(11): 3228-3237.
- Carrado, K.A., Thiyagarajan, P. and Song, K., 1997. A study of organo-hectorite clay crystallization. *Clay Minerals*, 32(1): 29-40.

- Carrado, K.A., Xu, L., D.M.G., K. Song, S. Seifert, A. and Botto, R.E., 2015. Crystallization of a Layered Silicate Clay as Monitored by Small-Angle X-ray Scattering and NMR. *Chemistry of Materials*, 12(10): 3052-3059.
- Carretero, M. I. (2002). Clay minerals and their beneficial effects upon human health. a review. *Applied Clay Science*, 21(3): 155-163.
- Chang, C.W., Spreeuwel, A.V., Zhang, C. and Varghese, S., 2010. PEG/clay nanocomposite hydrogel: a mechanically robust tissue engineering scaffold. *Soft Matter*, 6(20): 5157-5164.
- Chen, G., Li, D., Li, J., Cao, X., Wang, J., Shi, X. and Guo, R., 2015. Targeted doxorubicin delivery to hepatocarcinoma cells by lactobionic acid-modified laponite nanodisks. *New Journal of Chemistry*, 39(4): 2847-2855.
- Chen, W., Zhang, B., Mahony, T., Gu, W., Rolfe, B. and Xu, Z.P., 2016. Efficient and Durable Vaccine against Intimin β of Diarrheagenic E. Coli Induced by Clay Nanoparticles. *Small*, 12(12): 1627.
- Christidis, G. , Aldana, C. , Chryssikos, G. , Gionis, V. , Kalo, H. , Stöter, M., Breu, J., and Robert J., 2018. The nature of laponite: pure hectorite or a mixture of different trioctahedral phases? *Minerals*, 8(8).
- Cho, K.L., Hill, A.J., Caruso, F. and Kentish, S.E., 2015. Chlorine resistant glutaraldehyde crosslinked polyelectrolyte multilayer membranes for desalination. *Advanced Materials*, 27(17): 2791.
- Contin, A., Biffis, A., Sterchele, S., Dormbach, K., Schipmann, S. and Pich, A., 2014. Metal nanoparticles inside microgel/clay nanohybrids: Synthesis, characterization and catalytic efficiency in cross-coupling reactions. *J Colloid Interface Sci*, 414: 41-5.
- Cool, P. and Vansant, E.F., 1996. Preparation and characterization of zirconium pillared laponite and hectorite. *Microporous Materials*, 6(1): 27-36.
- Cummins, H.Z., 2007. Liquid, glass, gel: The phases of colloidal Laponite. *Journal of Non-Crystalline Solids*, 353(41-43): 3891-3905.
- Daab, M., Rosenfeldt, S., Kalo, H., Stöter, M., Bojer, B., Siegel, R., Forster, S., Senker, J. and Breu, J., 2017. Two-Step Delamination of Highly Charged, Vermiculite-like Layered Silicates via Ordered Heterostructures. *Langmuir*, 33(19): 4816-4822.
- Daniel, L.M., Frost, R.L. and Zhu, H.Y., 2008. Edge-modification of laponite with dimethyl-octylmethoxysilane. *J Colloid Interface Sci*, 321(2): 302-9.

1226 Dawson, J.I., Kanczler, J.M., Yang, X.B., Attard, G.S. and Oreffo, R.O., 2011. Clay gels for the
1227 delivery of regenerative microenvironments. *Adv Mater*, 23(29): 3304-8.

1228 Dawson, J.I. and Oreffo, R.O., 2013. Clay: new opportunities for tissue regeneration and biomaterial
1229 design. *Adv Mater*, 25(30): 4069-86.

1230 Decarreau, A., Grauby, O., & Petit, S. (1992). The actual distribution of octahedral cations in 2: 1 clay
1231 minerals: results from clay synthesis. *Applied Clay Science*, 7(1-3), 147-167.

1232 Decarreau, A., Vigier, N., Palkova, H., Petit, S., Vieillard, P. and Fontaine, C., 2012. Partitioning of
1233 lithium between smectite and solution: An experimental approach. *Geochimica et*
1234 *Cosmochimica Acta*, 85: 314-325.

1235 Decarreau A. 1980. Experimental crystallogenesi s of Mg-smectite:hectorite, stevensite. *Bull. Minéral.*
1236 103:579-590.

1237 Deepracha, S., Bureekaew, S., & Ogawa, M., 2019. Synergy effects of the complexation of a titania and
1238 a smectite on the film formation and its photocatalyst'performance. *Applied Clay Science*, 169,
1239 129-134.

1240 Delavernhe, L., Pilavtepe, M. and Emmerich, K., 2018. Cation exchange capacity of natural and
1241 synthetic hectorite. *Applied Clay Science*, 151: 175-180.

1242 Dimos, K., Arcudi, F., Kouloumpis, A., Koutselas, I.B., Rudolf, P., Gournis, D. and Prato, M., 2017.
1243 Top-down and bottom-up approaches to transparent, flexible and luminescent nitrogen-doped
1244 carbon nanodot-clay hybrid films. *Nanoscale*, 9(29): 10256-10262.

1245 Ding, L., Hu, Y., Luo, Y., Zhu, J., Wu, Y., Yu, Z., Cao, X., Peng, C., Shi, X. and Guo, R., 2016.
1246 LAPONITE(R)-stabilized iron oxide nanoparticles for in vivo MR imaging of tumors. *Biomater*
1247 *Sci*, 4(3): 474-82.

1248 Duque-Redondo, E., Manzano, H., Epelde-Elezcano, N., Martínez-Martínez, V. and López-Arbeloa, I.,
1249 2014. Molecular Forces Governing Shear and Tensile Failure in Clay-Dye Hybrid Materials.
1250 *Chemistry of Materials*, 26(15): 4338-4345.

1251 Dykes, L.M.C., Torkelson, J.M., Burghardt, W.R. and Krishnamoorti, R., 2010. Shear-induced
1252 orientation in polymer/clay dispersions via in situ X-ray scattering. *Polymer*, 51(21): 4916-4927.

1253 Elder, D.L., Benight, S.J., Song, J., Robinson, B.H. and Dalton, L.R., 2014. Matrix-Assisted Poling of
 1254 Monolithic Bridge-Disubstituted Organic NLO Chromophores. *Chemistry of Materials*, 26(2):
 1255 872–874.

1256 Fenero, M., Palenzuela, J., Azpitarte, I., Knez, M., Rodriguez, J. and Tena-Zaera, R., 2017.
 1257 Laponite-Based Surfaces with Holistic Self-Cleaning Functionality by Combining Antistatics
 1258 and Omniphobicity. *ACS Appl Mater Interfaces*, 9(44): 39078-39085.

1259 Finck, N., Dardenne, K. and Geckeis, H., 2015. Am(III) coprecipitation with and adsorption on the
 1260 smectite hectorite. *Chemical Geology*, 409: 12-19.

1261 Finck, N., Stumpf, T., Walther, C. and Bosbach, D., 2008. TRLFS characterization of Eu(III)-doped
 1262 synthetic organo-hectorite. *Journal of Contaminant Hydrology*, 102(3–4): 253-262.

1263 Franco, F., Pozo, M., Cecilia, J.A., Benítez-Guerrero, M. and Lorente, M., 2016. Effectiveness of
 1264 microwave assisted acid treatment on dioctahedral and trioctahedral smectites. The influence of
 1265 octahedral composition. *Applied Clay Science*, 120: 70-80.

1266 Fujimura, T., Ramasamy, E., Ishida, Y., Shimada, T., Takagi, S. and Ramamurthy, V., 2016. Sequential
 1267 energy and electron transfer in a three-component system aligned on a clay nanosheet. *Physical
 1268 Chemistry Chemical Physics Pccp*, 18(7): 5404.

1269 Gaharwar, A.K., Avery, R.K., Assmann, A., Paul, A., Mckinley, G.H., Khademhosseini, A. and Olsen,
 1270 B.D., 2014. Shear-thinning nanocomposite hydrogels for the treatment of hemorrhage. *Acs
 1271 Nano*, 8(10): 9833.

1272 Gaharwar, A.K., Mihaila, S.M., Swami, A., Patel, A., Sant, S., Reis, R.L., Marques, A.P., Gomes, M.E.
 1273 and Khademhosseini, A., 2013. Bioactive silicate nanoplatelets for osteogenic differentiation of
 1274 human mesenchymal stem cells. *Adv Mater*, 25(24): 3329-36.

1275 Gao, R., Fang, X. and Yan, D., 2018. Direct white-light emitting room-temperature-phosphorescence
 1276 thin films with tunable two-color polarized emission through orientational hydrogen-bonding
 1277 layer-by-layer assembly. *Journal of Materials Chemistry C*, 6(16): 4444-4449.

1278 Gonçalves, M., Figueira, P., Maciel, D., Rodrigues, J., Qu, X., Liu, C., Tomás, H. and Li, Y., 2014.
 1279 pH-sensitive Laponite®/doxorubicin/alginate nanohybrids with improved anticancer efficacy.
 1280 *Acta Biomaterialia*, 10(1): 300-7.

1281 González, B., da Silva, T.H., Ciuffi, K.J., Vicente, M.A., Trujillano, R., Rives, V., de Faria, E.H., Korili,
1282 S.A. and Gil, A., 2017. Laponite functionalized with biuret and melamine-Application to
1283 adsorption of antibiotic trimethoprim. *Microporous and Mesoporous Materials*, 253: 112-122.

1284 Grabolle, M., Starke, M. and Resch-Genger, U., 2016. Highly Fluorescent dye-nanoclay Hybrid
1285 Materials Made from Different Dye Classes. *Langmuir*, 32(14): 3506-13.

1286 Guerra, D.L., Airoidi, C., Lemos, V.P. and Angelica, R.S., 2008. Adsorptive, thermodynamic and
1287 kinetic performances of Al/Ti and Al/Zr-pillared clays from the Brazilian Amazon region for
1288 zinc cation removal. *J Hazard Mater*, 155(1-2): 230-42.

1289 Guerra, D.L., Airoidi, C. and Viana, R.R., 2010. Modification of hectorite by organofunctionalization
1290 for use in removing U(VI) from aqueous media: thermodynamic approach. *J Environ Radioact*,
1291 101(2): 122-33.

1292 Guerra, D.L., Santos, M.R.M.C. and Airoidi, C., 2009. Mercury adsorption on natural and
1293 organofunctionalized smectites - thermodynamics of cation removal. *Journal of the Brazilian*
1294 *Chemical Society*, 20(20): 594-603.

1295 Hai, C., Zhou, Y., Fuji, M., Shirai, T., Ren, X., Zeng, J. and Li, X., 2018a. Electrical conductivity of
1296 hydrothermally synthesized sodium lithium magnesium silicate. *Materials Research Bulletin*, 97:
1297 473-482.

1298 Hai, C., Zhou, Y., Wang, F. and Fuji, M., 2018b. Direct growth of lithium magnesium silicate
1299 nanotubes on a glass slide. *CrystEngComm*, 20(32): 4694-4701.

1300 Hashimoto, K., Irie, H., & Fujishima, A., 2005. TiO₂ photocatalysis: a historical overview and future
1301 prospects. *Japanese Journal of Applied Physics*, 44(12), 8269-8285.

1302 Hegyesi, N., Vad, R.T. and Pukánszky, B., 2017. Determination of the specific surface area of layered
1303 silicates by methylene blue adsorption: The role of structure, pH and layer charge. *Applied Clay*
1304 *Science*, 146: 50-55.

1305 Heinz, H., Vaia, R.A., Krishnamoorti, R., & Farmer, B. L., 2007. Self-Assembly of Alkylammonium
1306 Chains on Montmorillonite: Effect of Chain Length, Head Group Structure, and Cation
1307 Exchange Capacity. *Chemistry of Materials*, 19(1): 59-68.

- Herling, M.M., Kalo, H., Seibt, S., Schobert, R. and Breu, J., 2012. Tailoring the pore sizes of microporous pillared interlayered clays through layer charge reduction. *Langmuir*, 28(41): 14713-9.
- Higashi, S., Miki, H. and Komarneni, S., 2007. Mn-smectites: Hydrothermal synthesis and characterization. *Applied Clay Science*, 38(1-2): 104-112.
- Hill, E.H., Claes, N., Bals, S. and Liz-Marzán, L.M., 2016. Layered Silicate Clays as Templates for Anisotropic Gold Nanoparticle Growth. *Chemistry of Materials*, 28(14): 5131-5139.
- Hill, E.H., Zhang, Y. and Whitten, D.G., 2015. Aggregation of cationic p-phenylene ethynylenes on Laponite clay in aqueous dispersions and solid films. *J Colloid Interface Sci*, 449: 347-56.
- Hong, S., Sycks, D., Chan, H.F., Lin, S., Lopez, G.P., Guilak, F., Leong, K.W. and Zhao, X., 2015a. 3D Printing of Highly Stretchable and Tough Hydrogels into Complex, Cellularized Structures. *Adv Mater*, 27(27): 4035-40.
- Hong, S.H., Shin, M., Lee, J., Ryu, J.H., Lee, S., Yang, J.W., Kim, W.D. and Lee, H., 2015b. Stable Alginate Gel Prepared by Linkage Exchange from Ionic to Covalent Bonds. *Advanced Healthcare Materials*, 5(1): 75-79.
- Hoppe, A., Gldal, N.S. and Boccaccini, A.R., 2011. A review of the biological response to ionic dissolution products from bioactive glasses and glass-ceramics. *Biomaterials*, 32(11): 2757-74.
- Huang, X., Ivanova, N., Strzelec, A. and Zacharia, N.S., 2018. Assembly of large area crack free clay porous films. *RSC Advances*, 8(2): 1001-1004.
- Iwasaki, T., 1989. Rheological Properties of Organophilic Synthetic Hectorites and Saponites. *Clays & Clay Minerals*, 37(3): 248-257.
- Iwase, H. , Ogura, T. , Sakuma, H. , Tamura, K. , & Fukushima, Y. . 2018. Structural investigation of hectorite aqueous suspensions by dielectric microscopy and small-angle neutron scattering coupling with rheological measurement. *Applied Clay Science*, 157: 24-30.
- Jaber, M. and Mieh -Brendl , J., 2008. Synthesis, characterization and applications of 2:1 phyllosilicates and organophyllosilicates: Contribution of fluoride to study the octahedral sheet. *Microporous and Mesoporous Materials*, 107(1-2): 121-127.

1335 Ji, Y., Xie, W., Fan, Y., Shi, Y., Kong, D. and Lu, J., 2016. Degradation of trimethoprim by
 1336 thermo-activated persulfate oxidation: Reaction kinetics and transformation mechanisms.
 1337 Chemical Engineering Journal, 286: 16-24.

1338 Jin, Y., Shen, Y., Yin, J., Qian, J. and Huang, Y., 2018. Nanoclay-Based Self-Supporting Responsive
 1339 Nanocomposite Hydrogels for Printing Applications. ACS Appl Mater Interfaces, 10(12):
 1340 10461-10470.

1341 Josef, B., Seidl, W., Alexander J. Stoll, and, K.G.L. and Probst, T.U., 2001. Charge Homogeneity in
 1342 Synthetic Fluorohectorite. Chem. Mater(13): 4213-4220.

1343 Joshi, G.V., Pawar, R.R., Kevadiya, B.D. and Bajaj, H.C., 2011. Mesoporous synthetic hectorites: A
 1344 versatile layered host with drug delivery application. Microporous and Mesoporous Materials,
 1345 142(2-3): 542-548.

1346 Jung, H., Kim, H. Y., Hwang, S., & Choy, J. (2008). Laponite-based nanohybrid for enhanced solubility
 1347 and controlled release of itraconazole. Int J Pharm, 349(1), 283-290.

1348 Kalo, H., Milius, W. and Breu, J., 2012a. Single crystal structure refinement of one- and two-layer
 1349 hydrates of sodium fluorohectorite. RSC Advances, 2(22): 8452.

1350 Kalo, H., Moller, M.W., Kunz, D.A. and Breu, J., 2012b. How to maximize the aspect ratio of clay
 1351 nanoplatelets. Nanoscale, 4(18): 5633-9.

1352 Kalo, H., Möller, M.W., Ziadeh, M., Dolejš, D. and Breu, J., 2010. Large scale melt synthesis in an
 1353 open crucible of Na-fluorohectorite with superb charge homogeneity and particle size. Applied
 1354 Clay Science, 48(1-2): 39-45.

1355 Karmous, M.S., Ben Rhaïem, H., Robert, J.L., Lanson, B. and Ben Haj Amara, A., 2009. Charge
 1356 location effect on the hydration properties of synthetic saponite and hectorite saturated by Na⁺,
 1357 Ca²⁺ cations: XRD investigation. Applied Clay Science, 46(1): 43-50.

1358 Keeling, J. L., and Zhou, C. H., 2012. Clay research opportunities arising from increased trade between
 1359 china and south australia. China Non-Metallic Minerals Industry.

1360 Khan, F.-A., Vallat, A. and Süß-Fink, G., 2011. Highly selective low-temperature hydrogenation of
 1361 furfuryl alcohol to tetrahydrofurfuryl alcohol catalysed by hectorite-supported ruthenium
 1362 nanoparticles. Catalysis Communications, 12(15): 1428-1431.

1363 Khan, F.-A., Vallat, A. and Süss-Fink, G., 2012. Highly selective C=C bond hydrogenation in
 1364 α,β -unsaturated ketones catalyzed by hectorite-supported ruthenium nanoparticles. *Journal of*
 1365 *Molecular Catalysis A: Chemical*, 355: 168-173.

1366 Kolesky, D. B. , Truby, R. L. , Gladman, A. S. , Busbee, T. A. , Homan, K. A. , & Lewis, J. A.. 2014.
 1367 3D bioprinting of vascularized, heterogeneous cell-laden tissue constructs. *Advanced Materials*,
 1368 26(19): 3124-3130.

1369 Komadel, P., 2016. Acid activated clays: Materials in continuous demand. *Applied Clay Science*, 131:
 1370 84-99.

1371 Komadel, P., Janek, M., Madejová, J., Weekes, A. and Breen, C., 1997. Acidity and catalytic activity of
 1372 mildly acid-treated Mg-rich montmorillonite and hectorite. *J.chem.soc.faraday Trans*, 93(23):
 1373 4207-4210.

1374 Kotal, M. and Bhowmick, A.K., 2015. Polymer nanocomposites from modified clays: Recent advances
 1375 and challenges. *Progress in Polymer Science*, 51: 127-187.

1376 Lee B , Koo S., 2011. Preparation of silver nanoparticles on the surface of fine magnetite particles by a
 1377 chemical reduction[J]. *Journal of Industrial & Engineering Chemistry*, 17(4):762-766.

1378 Ley, C., Bordat, P., di Stefano, L.H., Remongin, L., Ibrahim, A., Jacques, P. and Allonas, X., 2015a.
 1379 Joint spectroscopic and theoretical investigation of cationic cyanine dye Astrazon Orange-R:
 1380 solvent viscosity controlled relaxation of excited states. *Phys Chem Chem Phys*, 17(8): 5982-90.

1381 Ley, C., Brendle, J., Miranda, M. and Allonas, X., 2017. Spectroscopic Studies of the Interactions
 1382 between a Cationic Cyanine Dye and a Synthetic Phyllosilicate: From Photophysics to Hybrid
 1383 Materials. *Langmuir*, 33(27): 6812-6818.

1384 Ley, C., Brendle, J., Walter, A., Jacques, P., Ibrahim, A. and Allonas, X., 2015b. On the interaction of
 1385 triarylmethane dye crystal violet with LAPONITE(R) clay: using mineral nanoparticles to
 1386 control the dye photophysics. *Phys Chem Chem Phys*, 17(26): 16677-81.

1387 Lezhnina, M.M., Grewe, T., Stoehr, H. and Kynast, U., 2012. Laponite Blue: Dissolving the Insoluble.
 1388 *Angewandte Chemie International Edition*, 51(42): 10652-10655.

1389 Li, K., Wang, S., Wen, S., Tang, Y., Li, J., Shi, X. and Zhao, Q., 2014. Enhanced In Vivo Antitumor
 1390 Efficacy of Doxorubicin Encapsulated within Laponite Nanodisks. *ACS Applied Materials &*
 1391 *Interfaces*, 6(15): 12328-12334.

1392 Li, Z., Hou, Z., Fan, H. and Li, H., 2017a. Organic-Inorganic Hierarchical Self-Assembly into Robust
 1393 Luminescent Supramolecular Hydrogel. *Advanced Functional Materials*, 27(2): 1604379.
 1394 Li, Z., Li, P., Xu, Q., and Li, H., 2015. Europium(III)- β -diketonate complex-containing nanohybrid
 1395 luminescent pH detector. *Chemical Communications*, 51(53): 10644-7.
 1396 Li, Z., Wang, G., Wang, Y. and Li, H., 2018. Reversible Phase Transition of Robust Luminescent
 1397 Hybrid Hydrogels. *Angew Chem Int Ed Engl*, 57(8): 2194-2198.
 1398 Li, Z., Zhang, Y.-M., Wang, H.-Y., Li, H. and Liu, Y., 2017b. Mechanical Behaviors of Highly Swollen
 1399 Supramolecular Hydrogels Mediated by Pseudorotaxanes. *Macromolecules*, 50(3): 1141-1146.
 1400 Liu, H., Gu, X., Hu, M., Hu, Y. and Wang, C., 2014a. Facile fabrication of nanocomposite
 1401 microcapsules by combining layer-by-layer self-assembly and Pickering emulsion templating.
 1402 *RSC Adv.*, 4(32): 16751-16758.
 1403 Liu, J., Liu, G., Zhang, M., Sun, P. and Zhao, H., 2013. Synthesis and Self-Assembly of Amphiphilic
 1404 Janus Laponite Disks. *Macromolecules*, 46(15): 5974-5984.
 1405 Liu, L.F., Cai, Z.B., Shen, J.N., Wu, L.X., Hoek, E.M.V. and Gao, C.J., 2014b. Fabrication and
 1406 characterization of a novel poly(amide-urethane@imide) TFC reverse osmosis membrane with
 1407 chlorine-tolerant property. *Journal of Membrane Science*, 469(6): 397-409.
 1408 Liu, Y. and Lee, B.P., 2016. Recovery property of double-network hydrogel containing mussel-inspired
 1409 adhesive moiety and nano-silicate. *Journal of Materials Chemistry B Materials for Biology &*
 1410 *Medicine*, 4(40): 6534-6540.
 1411 Liu, Y., Meng, H., Qian, Z., Fan, N., Choi, W., Zhao, F. and Lee, B.P., 2017. A moldable nanocomposite
 1412 hydrogel composed of a mussel-inspired polymer and a nanosilicate as a fit-to-shape tissue
 1413 sealant. *Angew Chem Int Ed Engl*, 56(15): 4224-4228.
 1414 Ma, J., Jia, Y., Jing, Y., Sun, J. and Yao, Y., 2009. Synthesis and photocatalytic activity of
 1415 TiO₂-hectorite composites. *Applied Clay Science*, 46(1): 114-116.
 1416 Ma, Y., Lin, M., Huang, G., Li, Y., Wang, S., Bai, G., Lu, T., and Xu, F. 2018. 3D Spatiotemporal
 1417 Mechanical Microenvironment: A Hydrogel- Based Platform for Guiding Stem Cell Fate.
 1418 *Advanced Materials*, 30(49): 1705911.
 1419 Makoto, O., Takayuki, M. and Tomohiko, O., 2008. Preparation of hectorite-like swelling silicate with
 1420 controlled layer charge density. *Journal of the Ceramic Society of Japan*.

- Min, J., Braatz, R.D. and Hammond, P.T., 2014. Tunable staged release of therapeutics from layer-by-layer coatings with clay interlayer barrier. *Biomaterials*, 35(8): 2507-17.
- Mishra, A.K., Chattopadhyay, S., Rajamohanan, P.R. and Nando, G.B., 2011. Effect of tethering on the structure-property relationship of TPU-dual modified Laponite clay nanocomposites prepared by ex-situ and in-situ techniques. *Polymer*, 52(4): 1071-1083.
- Möller, M.W., Hirsemann, D., Haarmann, F., Senker, J.r. and Breu, J., 2010. Facile Scalable Synthesis of Rectorites. *Chemistry of Materials*, 22(1): 186-196.
- Muller, F., Besson, G., Manceau, A. and Drits, V.A., 1997. Distribution of isomorphous cations within octahedral sheets in montmorillonite from Camp-Bertaux. *Physics & Chemistry of Minerals*, 24(3): 159-166.
- Naveau, E., Calberg, C., Detrembleur, C., Bourbigot, S., Jérôme, C. and Alexandre, M., 2009. Supercritical CO₂ as an efficient medium for layered silicate organomodification: Preparation of thermally stable organoclays and dispersion in polyamide 6. *Polymer*, 50(6): 1438-1446.
- Nennemann, A., Kulbach, S. and Lagaly, G., 2001. Entrapping pesticides by coagulating smectites. *Applied Clay Science*, 18(5): 285-298.
- Norma, N.H., Jeanmarie, L., Jeanluc, P., Laurent, D. and Elodie, B., 2004. Aqueous Dispersions of Silane-Functionalized Laponite Clay Platelets. A First Step toward the Elaboration of Water-Based Polymer/Clay Nanocomposites. *Langmuir*, 20(5): 1564-1571.
- Okada T., Matsutomo T., and Ogawa M., 2010. Nanospace Engineering of Methylviologen Modified Hectorite-Like Layered Silicates with Varied Layer Charge Density for the Adsorbents Design. *J. Phys. Chem. C*, 539-545.
- Okada, T., Kobari, H. and Haeiwa, T., 2016a. Effects of fluoride and urea on the crystal growth of a hectorite-like layered silicate on a silica surface. *Applied Clay Science*, 132-133: 320-325.
- Okada, T., Kumasaki, A., Shimizu, K., Yamagishi, A. and Sato, H., 2016b. Application of Hectorite-Coated Silica Gel Particles as a Packing Material for Chromatographic Resolution. *J Chromatogr Sci*, 54(7): 1238-43.
- Okada, T. and Ogawa, M., 2003. 1,1'-Dimethyl-4,4'-bipyridinium-smectites as a novel adsorbent of phenols from water through charge-transfer interactions. *Chemical Communications*, 9(12): 1378.

- Okada, T., Sueyoshi, M. and Minamisawa, H.M., 2015a. In Situ Crystallization of Al-Containing Silicate Nanosheets on Monodisperse Amorphous Silica Microspheres. *Langmuir*, 31(51): 13842-9.
- Okada, T., Suzuki, A., Yoshido, S. and Minamisawa, H.M., 2015b. Crystal architectures of a layered silicate on monodisperse spherical silica particles cause the topochemical expansion of the core-shell particles. *Microporous and Mesoporous Materials*, 215: 168-174.
- Okada, T., Yoshido, S., Miura, H., Yamakami, T., Sakai, T. and Mishima, S., 2012. Swellable Microsphere of a Layered Silicate Produced by Using Monodispersed Silica Particles. *The Journal of Physical Chemistry C*, 116(41): 21864-21869.
- Okay, O., 2011. DNA hydrogels: New functional soft materials. *Journal of Polymer Science Part B Polymer Physics*, 49(8): 551-556.
- Osman, A.F., Edwards, G.A., Schiller, T.L., Andriani, Y., Jack, K.S., Morrow, I.C., Halley, P.J. and Martin, D.J., 2012. Structure–Property Relationships in Biomedical Thermoplastic Polyurethane Nanocomposites. *Macromolecules*, 45(1): 198-210.
- Pardhy, N.P. and Budhlall, B.M., 2010. Pickering emulsion as a template to synthesize Janus colloids with anisotropy in the surface potential. *Langmuir*, 26(16): 13130-41.
- Patro, T.U. and Wagner, H.D., 2011. Layer-by-layer assembled PVA/Laponite multilayer free-standing films and their mechanical and thermal properties. *Nanotechnology*, 22(45): 455706.
- Patro, T.U. and Wagner, H.D., 2016. Influence of graphene oxide incorporation and chemical cross-linking on structure and mechanical properties of layer-by-layer assembled poly(Vinyl alcohol)-Laponite free-standing films. *Journal of Polymer Science Part B: Polymer Physics*, 54(22): 2377-2387.
- Pawar, R.R., Kevadiya, B.D., Brahmabhatt, H. and Bajaj, H.C., 2013. Template free synthesis of mesoporous hectorites: efficient host for pH responsive drug delivery. *Int J Pharm*, 446(1-2): 145-52.
- Pawar, R.R., Lalhmunsiam, Gupta, P., Sawant, S.Y., Shahmoradi, B. and Lee, S.M., 2018. Porous synthetic hectorite clay-alginate composite beads for effective adsorption of methylene blue dye from aqueous solution. *International Journal of Biological Macromolecules*, 114: 1315.

- Pawar, R.R., Patel, H.A., Sethia, G. and Bajaj, H.C., 2009. Selective adsorption of carbon dioxide over nitrogen on calcined synthetic hectorites with tailor-made porosity. *Applied Clay Science*, 46(1): 109-113.
- Petit S., Righi D., Decarreau A. 2008. Transformation of synthetic Zn-stevensite to Zn-talc induced by the Hofmann-Klemen effect. *Clays and Clay Min.*, 56, 645-654.
- Pedron, S., Becka, E., & Harley, B. A. 2015. Spatially gradated hydrogel platform as a 3D engineered tumor microenvironment. *Advanced Materials*, 27(9): 1567-1572.
- Phothitontimongkol, T., Sanuwong, K., Siebers, N., Sukpirom, N. and Unob, F., 2013. Functionalized hectorite clay mineral for Ag(I) ions extraction from wastewater and preparation of silver nanoparticles supported clay. *Applied Clay Science*, 80-81: 346-350.
- Phothitontimongkol, T., Siebers, N., Sukpirom, N. and Unob, F., 2009. Preparation and characterization of novel organo-clay minerals for Hg(II) ions adsorption from aqueous solution. *Applied Clay Science*, 43(3-4): 343-349.
- Phuoc, T.X., Howard, B.H. and Chyu, M.K., 2009. Synthesis and rheological properties of cation-exchanged Laponite suspensions. *Colloids and Surfaces A: Physicochemical and Engineering Aspects*, 351(1-3): 71-77.
- Priolo, M.A., Holder, K.M., Greenlee, S.M., Stevens, B.E. and Grunlan, J.C., 2013. Precisely Tuning the Clay Spacing in Nanobrick Wall Gas Barrier Thin Films. *Chemistry of Materials*, 25(9): 1649-1655.
- Pujala, R.K., Schneijdenberg, C., van Blaaderen, A. and Bohidar, H.B., 2018. In-situ Observation of Hierarchical Self-Assembly Driven by Bicontinuous Gelation in Mixed Nanodisc Dispersions. *Sci Rep*, 8(1): 5589.
- Raeburn, J., Zamith, C.A. and Adams, D.J., 2013. The importance of the self-assembly process to control mechanical properties of low molecular weight hydrogels. *Chemical Society Reviews*, 42(12): 5143-56.
- Rajesh, S., Zhao, Y., Fong, H. and Menkhaus, T.J., 2017. Nanofiber multilayer membranes with tailored nanochannels prepared by molecular layer-by-layer assembly for high throughput separation. *J. Mater. Chem. A*, 5(9): 4616-4628.

Robertson, J. and Bandosz, T.J., 2006. Photooxidation of dibenzothiophene on TiO₂/hectorite thin films layered catalyst. *J Colloid Interface Sci*, 299(1): 125-35.

Sánchez, T., Gebretsadik, F.B., Salagre, P., Cesteros, Y., Guillén-Hurtado, N., García-García, A. and Bueno-López, A., 2013a. Evaluation of hectorites, synthesized in different conditions, as soot combustion catalysts after impregnation with copper. *Applied Clay Science*, 77-78: 40-45.

Sánchez, T., Salagre, P. and Cesteros, Y., 2013b. Ultrasounds and microwave-assisted synthesis of mesoporous hectorites. *Microporous and Mesoporous Materials*, 171: 24-34.

Sánchez, T., Salagre, P., Cesteros, Y. and Bueno-López, A., 2012. Use of delaminated hectorites as supports of copper catalysts for the hydrogenolysis of glycerol to 1,2-propanediol. *Chemical Engineering Journal*, 179: 302-311.

Sawant, S.Y., Pawar, R.R., Somani, R.S. and Bajaj, H.C., 2014. Facile hard template approach for synthetic hectorite hollow microspheres. *Materials Letters*, 128: 121-124.

Schoonheydt, R.A., 1991. Clay Adsorbed Dyes: Methylene Blue on Laponite. *Clay Minerals*, 27(1): 91-100.

Sethia, G., Patel, H.A., Pawar, R.R. and Bajaj, H.C., 2014. Porous synthetic hectorites for selective adsorption of carbon dioxide over nitrogen, methane, carbon monoxide and oxygen. *Applied Clay Science*, 91-92: 63-69.

Shi, L., Xu, Y. and Li, Q., 2008. Controlled Growth of Lead Oxide Nanosheets, Scrolled Nanotubes, and Nanorods. *Crystal Growth & Design*, 8(10): 3521-3525.

Spagnuolo, M., 2004. Coprecipitation of trace metal ions during the synthesis of hectorite. *Applied Clay Science*, 27(3-4): 129-140.

Staniford, M.C., Lezhnina, M.M., Gruener, M., Stegemann, L., Kuczius, R., Bleicher, V., Strassert, C.A. and Kynast, U.H., 2015. Photophysical efficiency-boost of aqueous aluminium phthalocyanine by hybrid formation with nano-clays. *Chemical Communications*, 51(70): 13534-13537.

Stocker, M., Seidl, W., Seyfarth, L., Senker, J. and Breu, J., 2008. Realisation of truly microporous pillared clays. *Chem Commun (Camb)*(5): 629-31.

Storaro, L., Lenarda, M., Ganzerla, R. and Rinaldi, A., 1996. Preparation of hydroxy Al and Al/Fe pillared bentonites from concentrated clay suspensions. *Microporous Materials*, 6(2): 55-63.

1534 Stöter, M., Biersack, B., Reimer, N., Herling, M., Stock, N., Schobert, R. and Breu, J., 2014. Ordered
 1535 Heterostructures of Two Strictly Alternating Types of Nanoreactors. *Chemistry of Materials*,
 1536 26(18): 5412-5419.

1537 Stöter, M., Biersack, B., Rosenfeldt, S., Leidl, M.J., Kalo, H., Schobert, R., Yersin, H., Ozin, G.A.,
 1538 Förster, S. and Breu, J., 2015. Encapsulation of functional organic compounds in nanoglass for
 1539 optically anisotropic coatings. *Angewandte Chemie*, 54(16): 4963-7.

1540 Stöter, M., Godrich, S., Feicht, P., Rosenfeldt, S., Thurn, H., Neubauer, J.W., Seuss, M., Lindner, P.,
 1541 Kalo, H., Moller, M., Fery, A., Förster, S., Papastavrou, G. and Breu, J., 2016. Controlled
 1542 Exfoliation of Layered Silicate Heterostructures into Bilayers and Their Conversion into Giant
 1543 Janus Platelets. *Angew Chem Int Ed Engl*, 55(26): 7398-402.

1544 Stöter, M., Kunz, D.A., Schmidt, M., Hirsemann, D., Kalo, H., Putz, B., Senker, J. and Breu, J., 2013.
 1545 Nanoplatelets of sodium hectorite showing aspect ratios of approximately 20,000 and superior
 1546 purity. *Langmuir*, 29(4): 1280-5.

1547 Strese, H. and Hofmann, U., 1941. Synthese von Magnesiumsilikat-Gelen mit zweidimensional
 1548 regelmäßiger struktur. *Zeitschrift Für Anorganische Und Allgemeine Chemie*, 247.

1549 Such, G.K., Quinn, J.F., Quinn, A., Tjipto, E. and Caruso, F., 2006. Assembly of ultrathin polymer
 1550 multilayer films by click chemistry. *Journal of the American Chemical Society*, 128(29):
 1551 9318-9319.

1552 Sudha, J.D., Pich, A., Reena, V.L., Sivakala, S. and Adler, H.-J.P., 2011. Water-dispersible
 1553 multifunctional polyaniline-laponite-keggin iron nanocomposites through a template approach.
 1554 *Journal of Materials Chemistry*, 21(41): 16642.

1555 Sun, B., Khan, F.-A., Vallat, A. and Süss-Fink, G., 2013. NanoRu@hectorite: A heterogeneous catalyst
 1556 with switchable selectivity for the hydrogenation of quinoline. *Applied Catalysis A: General*,
 1557 467: 310-314.

1558 Süss-Fink, G., Khan, F.A., Boudon, J. and Spassov, V., 2009. Shape- and Size-Selective Preparation of
 1559 Hectorite-Supported Ruthenium Nanoparticles for the Catalytic Hydrogenation of Benzene.
 1560 *Journal of Cluster Science*, 20(2): 341-353.

1561 Süss-Fink, G., Mollwitz, B., Therrien, B., Dadras, M., Laurenczy, G., Meister, A. and Meister, G., 2006.
 1562 Ruthenium Nanoparticles Intercalated in Hectorite: A Reusable Hydrogenation Catalyst for
 1563 Benzene and Toluene. *Journal of Cluster Science*, 18(1): 87-95.

1564 Suzuki, Y., Tenma, Y., Nishioka, Y., Kamada, K., Ohta, K. and Kawamata, J., 2011. Efficient
 1565 Two-Photon Absorption Materials Consisting of Cationic Dyes and Clay Minerals. *Journal of*
 1566 *Physical Chemistry C*, 115(42): 20653–20661.

1567 Szöllösi, G., Gombkötő, D., Mogyorós, A.Z. and Fülöp, F., 2018. Surface-Improved Asymmetric
 1568 Michael Addition Catalyzed by Amino Acids Adsorbed on Laponite. *Advanced Synthesis &*
 1569 *Catalysis*, 360(10): 1992-2004.

1570 Takagi, S., Shimada, T., Ishida, Y., Fujimura, T., Masui, D., Tachibana, H., Eguchi, M. and Inoue, H.,
 1571 2013. Size-matching effect on inorganic nanosheets: control of distance, alignment, and
 1572 orientation of molecular adsorption as a bottom-up methodology for nanomaterials. *Langmuir*
 1573 *the Acs Journal of Surfaces & Colloids*, 29(7): 2108-19.

1574 Takahashi, T., Yamada, Y., Kataoka, K. and Nagasaki, Y., 2005. Preparation of a novel PEG-clay hybrid
 1575 as a DDS material: dispersion stability and sustained release profiles. *Journal of Controlled*
 1576 *Release Official Journal of the Controlled Release Society*, 107(3): 408-16.

1577 Tan, H., Liu, W., Yu, D., Li, H., Hubbe, M.A., Gong, B., Zhang, W., Wang, H. and Li, G., 2014.
 1578 ASA-in-water emulsions stabilized by laponite nanoparticles modified with
 1579 tetramethylammonium chloride. *Chemical Engineering Science*, 116: 682-693.

1580 Tang, Y., Hill, E. H., Zhou, Z., Evans, D. G., Schanze, K. S., & Whitten, D. G. (2011). Synthesis,
 1581 self-assembly, and photophysical properties of cationic oligo(p-phenyleneethynylene)s.
 1582 *Langmuir*, 27(8), 4945-4955.

1583 Thien, B., Godon, N., Hubert, F. and Angéli, F., 2010. Structural identification of a trioctahedral
 1584 smectite formed by the aqueous alteration of a nuclear glass. *Applied Clay Science*, 49(3):
 1585 135-141.

1586 Tkáč, I., 1994. Acid-Treated Montmorillonites—A Study by ²⁹Si and ²⁷Al MAS NMR. *Clay Minerals*,
 1587 29(1): 11-19.

1588 Tokieda, D., Tsukamoto, T., Ishida, Y., Ichihara, H., Shimada, T. and Takagi, S., 2017. Unique
 1589 fluorescence behavior of dyes on the clay minerals surface: Surface Fixation Induced Emission
 1590 (S-FIE). *Journal of Photochemistry & Photobiology A Chemistry*, 339: 67-79.
 1591 Tomohiko, O. , Mutsuki, O. , Kazuki, T. , Tomohiko, Y. , & Hisako, S., 2018. Variation in thickness of a
 1592 layered silicate on spherical silica particles affected hplc chiral chromatographic resolution.
 1593 *Applied Clay Science*, 163:72-80.
 1594 Topuz, F. , Bartneck, M. , Pan, Y. , & Tacke, F. . 2017. One-step fabrication of biocompatible
 1595 multifaceted nanocomposite gels and nanolayers. *Biomacromolecules*, 18(2): 386-397.
 1596 Trikitiwong, P., Sukpirom, N., Shimazu, S. and Chavasiri, W., 2014. Iron oxide-pillared clay catalyzed
 1597 the synthesis of acetonides from epoxides. *Catalysis Communications*, 54: 104-107.
 1598 Tsapatsis, M. and Maheshwari, S., 2008. Pores by pillaring: not always a maze. *Angew Chem Int Ed*
 1599 *Engl*, 47(23): 4262-3.
 1600 Tsukamoto, T., Shimada, T. and Takagi, S., 2015. Structure resembling effect of clay surface on
 1601 photochemical properties of meso-phenyl or pyridyl-substituted monocationic antimony(V)
 1602 porphyrin derivatives. *Rsc Advances*, 5(11): 8479-8485.
 1603 Tzitzios, V., Basina, G., Bakandritsos, A., Hadjipanayis, C.G., Mao, H., Niarchos, D., Hadjipanayis,
 1604 G.C., Tucek, J. and Zboril, R., 2010. Immobilization of magnetic iron oxide nanoparticles on
 1605 laponite discs – an easy way to biocompatible ferrofluids and ferrogels. *Journal of Materials*
 1606 *Chemistry*, 20(26): 5418-5428.
 1607 Uzumcu, A.T., Guney, O. and Okay, O., 2016. Nanocomposite DNA hydrogels with temperature
 1608 sensitivity. *Polymer*, 100: 169-178.
 1609 Uzumcu, A.T., Guney, O. and Okay, O., 2018. Highly Stretchable DNA/Clay Hydrogels with
 1610 Self-Healing Ability. *ACS Appl Mater Interfaces*, 10(9): 8296-8306.
 1611 Varade, D. and Haraguchi, K., 2014. Novel bimetallic core-shell nanocrystal-clay composites with
 1612 superior catalytic activities. *Chem Commun (Camb)*, 50(23): 3014-7.
 1613 Velasco, J.I., Antunes, M., Ayyad, O., López-Cuesta, J.M., Gaudon, P., Saiz-Arroyo, C.,
 1614 Rodríguez-Pérez, M.A. and Saja, J.A.D., 2007. Foaming behaviour and cellular structure of
 1615 LDPE/hectorite nanocomposites. *Polymer*, 48(7): 2098-2108.

1616 Vicente, I., Salagre, P. and Cesteros, Y., 2010. Preparation of pure hectorite using microwaves. *Physics*
1617 *Procedia*, 8: 88-93.

1618 Vicente, I., Salagre, P., Cesteros, Y., Guirado, F., Medina, F. and Sueiras, J., 2009. Fast microwave
1619 synthesis of hectorite. *Applied Clay Science*, 43(1): 103-107.

1620 Wagner, H.D., 2007. Nanocomposites: paving the way to stronger materials. *Nature Nanotechnology*,
1621 2(12): 742-4.

1622 Wang, B., Zhou, M., Rozynek, Z. and Fossum, J.O., 2009. Electrorheological properties of organically
1623 modified nanolayered laponite: influence of intercalation, adsorption and wettability. *Journal of*
1624 *Materials Chemistry*, 19(13): 1816.

1625 Wang, J., Lin, L., Cheng, Q. and Jiang, L., 2012. A strong bio-inspired layered PNIPAM-clay
1626 nanocomposite hydrogel. *Angew Chem Int Ed Engl*, 51(19): 4676-80.

1627 Wang, J., Wheeler, P.A., Jarrett, W.L. and Mathias, L.J., 2007. Synthesis and characterization of dual-
1628 functionalized laponite clay for acrylic nanocomposites. *Journal of Applied Polymer Science*,
1629 106(3): 1496-1506.

1630 Wang, Q., Mynar, J.L., Yoshida, M., Lee, E., Lee, M., Okuro, K., Kinbara, K. and Aida, T., 2010.
1631 High-water-content mouldable hydrogels by mixing clay and a dendritic molecular binder.
1632 *Nature*, 463(7279): 339-43.

1633 Wang, S., Wu, Y., Guo, R., Huang, Y., Wen, S., Shen, M., Wang, J. and Shi, X., 2013. Laponite
1634 nanodisks as an efficient platform for Doxorubicin delivery to cancer cells. *Langmuir*, 29(16):
1635 5030-6.

1636 Wheeler, P.A., Wang, J., James Baker, A. and Mathias, L.J., 2005. Synthesis and Characterization of
1637 Covalently Functionalized Laponite Clay. *Chemistry of Materials*, 17(11): 3012-3018.

1638 Wu, Y., Guo, R., Wen, S., Shen, M., Zhu, M., Wang, J. and Shi, X., 2014. Folic acid-modified laponite
1639 nanodisks for targeted anticancer drug delivery. *J. Mater. Chem. B*, 2(42): 7410-7418.

1640 Xiao, S., Castro, R., Maciel, D., Goncalves, M., Shi, X., Rodrigues, J. and Tomas, H., 2016. Fine
1641 tuning of the pH-sensitivity of laponite-doxorubicin nanohybrids by polyelectrolyte multilayer
1642 coating. *Mater Sci Eng C Mater Biol Appl*, 60: 348-356.

1643 Xu, F., Liu, M., Li, X., Xiong, Z., Cao, X., Shi, X. and Guo, R., 2018. Loading of Indocyanine Green
 1644 within Polydopamine-Coated Laponite Nanodisks for Targeted Cancer Photothermal and
 1645 Photodynamic Therapy. *Nanomaterials (Basel)*, 8(5).

1646 Yang, Y., Liu, Z., Wu, D., Wu, M., Tian, Y., Niu, Z. and Huang, Y., 2013. Edge-modified amphiphilic
 1647 Laponite nano-discs for stabilizing Pickering emulsions. *J Colloid Interface Sci*, 410: 27-32.

1648 Yang, Y. and Zhang, J., 2018. Highly Stable Lithium-Sulfur Batteries Based on Laponite
 1649 Nanosheet-Coated Celgard Separators. *Advanced Energy Materials*, 8(25): 1801778.

1650 Yang, X. , Ke, X. , Yang, D. , Liu, J. , Guo, C. , Frost, R. , Su, H. , Zhu, H. , 2010. Effect of ethanol
 1651 washing of titania clay mineral composites on photocatalysis for phenol decomposition. *Applied*
 1652 *Clay Science*, 49(1-2), 0-50.

1653 Yao, Y., Jia, Y.Z., Sun, J.H., Jing, Y., Li, W., The method of using natural brine to synthesize
 1654 magnesium lithium silicate montmorillonite. Patent Number: ZL 200510096406.5

1655 Yoon, K., Hsiao, B.S. and Chu, B., 2008. Functional nanofibers for environmental applications. *Journal*
 1656 *of Materials Chemistry*, 18(44): 5326-5334.

1657 Yu, L. and Cebe, P., 2009. Crystal polymorphism in electrospun composite nanofibers of
 1658 poly(vinylidene fluoride) with nanoclay. *Polymer*, 50(9): 2133-2141.

1659 Yu, W. H., Ren, Q. Q., Tong, D. S., Zhou, C. H., & Hao, W. 2014. Clean production of
 1660 ctab-montmorillonite: formation mechanism and swelling behavior in xylene. *Applied Clay*
 1661 *Science*, 97-98(8), 222-234.

1662 Yue, D., Jing, Y., Ma, J., Xia, C., Yin, X. and Jia, Y., 2011. Removal of Neutral Red from aqueous
 1663 solution by using modified hectorite. *Desalination*, 267(1): 9-15.

1664 Yurekli, K., Conley, E. and Krishnamoorti, R., 2005. Effect of Laponite and a nonionic polymer on the
 1665 absorption character of cationic dye solutions. *Langmuir the Acs Journal of Surfaces & Colloids*,
 1666 21(13): 5825-30.

1667 Zhang, D., Zhou, C. H., Lin, C. X., Tong, D. S., & Yu, W. H. 2010. Synthesis of clay minerals. *Applied*
 1668 *Clay Science*, 50(1), 0-11.

1669 Zhao, L.Z., Zhou, C.H., Wang, J., Tong, D.S., Yu, W.H. and Wang, H., 2015. Recent advances in clay
 1670 mineral-containing nanocomposite hydrogels. *Soft Matter*, 11(48): 9229-46.

- Zhou, C. H. , Tong, D. , & Li, X. . 2010. Synthetic Hectorite: Preparation, Pillaring and Applications in Catalysis. Pillared Clays and Related Catalysts. Springer New York.
- Zhu, H. Y. , Zhao, J. C. , Liu, J. W. , Yang, X. Z. , & Shen, Y. N. , 2006. General synthesis of a mesoporous composite of metal oxide and silicate nanoparticles from a metal salt and laponite suspension for catalysis. Chemistry of Materials, 18(17), 3993-4001.
- Zhu, H. Y., Orthman, J. A., Li, J. Y., Zhao, J. C., Churchman, G. J., & Vansant, E. F., 2002. Novel composites of TiO₂ (anatase) and silicate nanoparticles. Chemistry of materials, 14(12), 5037-5044.
- Zhuang, Y., Zhao, L., Zheng, L., Hu, Y., Ding, L., Li, X., Liu, C., Zhao, J., Shi, X. and Guo, R., 2017. LAPONITE-Polyethylenimine Based Theranostic Nanoplatform for Tumor-Targeting CT Imaging and Chemotherapy. ACS Biomaterials Science & Engineering, 3(3): 431-442.